COLLOIDAL DEPOSITION VERSUS SHEAR AND POLYMER/SURFACTANT COMPOSITION

by
Lechuan Zhang

A thesis submitted to Johns Hopkins University in conformity with the requirements for

the degree of Master of Science in Engineering

Baltimore, Maryland
May 2020

ABSTRACT

Deposition and detachment of silica particles on glass substrate in presence of oppositely charged polymer/surfactant(P/S) were directly observed under diluting shear flow using flow cell apparatus and video microscopy. The hydrodynamic mechanism for deposition under a ramping shear flow was studied for evaluating lateral adhesion of particles. In experiments, all particles were initially deposited in a quiescent fluid mediated by synergistic P/S complex (acrylamide-acrylamidopropyltrimonium copolymer (AAC) & sodium lauryl ether sulfate (SLES)). However, these particles can be washed off partially by ramping shear flow. At a certain timepoint, the detachment would seize and most detached particles near substrate would redeposit. This timepoint is found to be simultaneous with local dilution under different conditions. A preferential dilution for surfactant in adsorbed layer is surmised to be responsible for this phenomenon. After dilution, polymer would stay adsorbed and regain available charges from surfactant. Stiffer bridges could form to seize further detachment and redeposit detached particles. Apart from the role of dilution in compensating final percent deposition, initial composition of P/S also has great impact by determining percent detachment before dilution, which was found to have a non-monotonic dependence on concentration of polymer. These findings illustrate the mechanism of particle deposition under a shear flow and the effect of both dilution and P/S composition in determining final percent deposition, which is important to optimizing delivery efficiency in multi-component formulation applications.

Primary Reader and Advisor: Michael A. Bevan

Secondary Reader: Joelle Frechette

ACKNOWLEDGMENTS

I would like to thank my advisor, Dr. Michael A. Bevan, who introduced me to the world of colloid. He taught me how to think like a scientist and solve problems like an engineer. I am grateful for the opportunity to conduct experiments and simulations in this an interesting and valuable project, and for the faith Dr. Bevan had in me to continue guiding me in my coming Ph.D. program.

I would also like to thank Dr. Joelle Frechette, for her course was inspiring to my research. I very much appreciate the help of past and current Bevan group members. I want to thank Dr. Helya Najafi for tutoring me experimental techniques and pioneered a lot of experimental work. I appreciate the discussion with Dr. Iassc Torres-Diaz on fluid mechanics. I want to thank Eugénie Jumai'an and Rachel Stein for discussions and helping me assimilate into American culture. I am grateful to Dennis Neibloom and Jianli Zhang for offering suggestions on this project.

I wholeheartedly thank my parents Xiufen Zhang and Jian Zhang for their support. I would also like to thank my friend Mo Yang for his influence on my critical thinking.

CONTENTS

LIST OF TABLES

LIST OF FIGURES

1. INTRODUCTION

1.1. Significance

Deposition of colloids from complex fluid has various applications in biological systems, oil and mining industries, pharmaceutical and personal care product[1]. Deposited colloids are often inevitably exposed to shear flow in such systems. In absence of lateral adhesion, they can be easily removed from surface. Complex formulation containing polymer, surfactant or protein is often added to strengthen the adhesion of particle on substrate.[2, 3] Such formulation could induce normal colloidal forces, yet lateral adhesion cannot be guaranteed. As dilution happens in complex fluid, formulation providing normal adhesion could be washed off. Currently, robust and efficient deposition under complicated fluid condition still remains challenging. Understanding how shear rate, dilution and composition affects deposition is essential to increase delivery ratio and best utilize each component in complex fluid.

1.2. Background

To increase percent deposition under shear flow, mechanism for deposition should be understood. Shear could induce a torque, a lateral force and a lifting force on center of particle[4, 5] that all could result in detachment via, respectably, rolling, sliding and lifting[6]. Normally, deposition mechanism could be categorized into two cases, through normal adhesion or lateral adhesion. In the case of deposition by normal adhesion, deformation and roughness of both particle[7-9] and surface[10-12] have been widely studied in biological and material system and proved to play a key role in deposition. Deformation and roughness could move pivot from particle center to the edge of contact and generate force lever for normal adhesive force to resist torque by shear flow. While friction between surfaces is the only force to resist shear induced lateral force, such

mechanism usually cannot resist high shear rate up to few thousand reciprocal second. Lateral adhesion is often a result of ligand-receptor bonding under shear flow that commonly seen in biomedical applications.[13, 14] Polyelectrolyte as a synthetic non-specific binding agent has also been studied as a mimic of ligand-receptor bonding and as a common depositing additive in personal care product.[15, 16] Since such tethers orient against flow and points towards substrate, they could provide extra lateral and normal force. Theoretically they could bring additional resistance against detachment.

Polymer is often added in personal care product such as shampoo as strong adhesive additive to deposit anionic capsules or micelles containing fragrance oil or silicon oil to perfume and condition hair. The main purpose of shampoo and other personal care product is to clean the surfaces. Excess amount of anionic surfactant is added in formulation and inevitably neutralize cationic polymer. The interaction between polymer/surfactant (P/S) complex and their synergistic effect on colloid deposition in quiescent fluid has been reviewed and studied.[17] The question remains how an external field such as shear flow could affect interaction between P/S in bulk and on substrate. Studies on the impact of shear flow on adsorbed polymer layer under a variety of solution condition, including shear rate[18], solvent power[19], ionic strength[20] and pH[21], have shown that adsorbed polymer layer can be significantly compressed under shear flow. Because of the strong electrostatic interaction between P/S, the complex often processes a stable yet not thermodynamic stable configuration especially at coacervation region while net charge is roughly neutral. Under shear flow, the coacervates would orient along flow direction.[22, 23] This is claimed to be a result of distortion of polymer chain by shear flow, which enhances interchange of surfactant between polymer chains.[24] Such reconfiguration drives complex towards a more thermodynamically stable state and larger size of coacervate. On the substrate, transfer of

surfactant in polymer layer was also observed to be enhanced increasingly with higher shear rate.[25]

Studies focusing on deposition mediated with P/S usually focuses the role of formulation by studying equilibrated mixture sample. However, dilution process is often inseparable in application with such formulation, such as shampoo. There are limited studies studying how dilution of P/S would affect deposition of colloid. In bulk phase, dilution of concentrated P/S (with ratio close to 1) is reported to be accompanied by percipition.[26, 27] Dilution decreases ionic strength and weakens screening effect between oppositely charged P/S. Interaction between P/S increases and solubility of complexes decreases. On a swift dilution, interface across concentration gradient could be densely packed and act as a kinetic barrier to slower exchange process between concentrated and diluted phase.[27] Dilution in the bulk phase could also significantly affect the adsorbed phase. Since the presence of surfactant swells adsorbed polymer layer, the observed increasing in adsorbed amount together with increased density indicate a preferential dilution of surfactant.[28-31] After dilution, polymer layer stays deposited and is almost free of oppositely charged surfactant. Polymer regains original charges and has more sites to form bridges with surfaces. This feature enables deposition of loaded capsules or micelles to be deposited on skin or hair.[32-35]

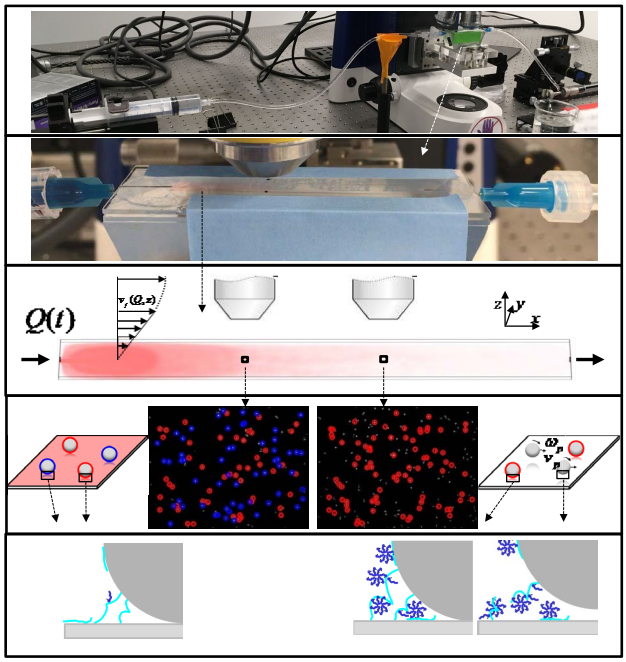

Figure 1. Illustration of flow cell experiment on multiple scales. (A) Setup of flow cell apparatus. (B) Flow chamber with injection of dyed diluting fluid. (C) Dilution profile near substrate chosen when solution is diluted in left window but not the right. (D) Particle scale schematics and tracked video of particle deposition behavior after(left) and before(right) dilution. Detached particles(grey) are not highlighted, deposited particles are highlighted and categorized into constantly deposited(red) and redeposited(blue). (E) Molecular scale schematics of particles near substrate after and before dilution. Size of polymer(cyan) and surfactant(blue) are extravagated to show composition difference.

1.3. Objective

In our recent work,[17] we studied the synergistic effect of polymer/surfactant on deposition of silica particles at a quiescent equilibrium state. Since the application of such system often involves diluting shear flow, in this paper, flow cell apparatus and video microscopy are used to directly measure particle deposition under different dilution, shear flow and composition condition. Realistic formulation composition and its diluted composition were investigated on silica colloid and glass slides system, which were proved to be two surrogates for commercial fragrant oil carrying capsules[36] and hair[37]. Initially deposited particles and particles deposited from flow were tracked and counted as a function of time or local concentration. Shear rate and concentration profile were obtained from simulation and related to deposition behavior. By comparing particle velocity with theoretical and performing force analysis, we calculated the lateral adhesive force on

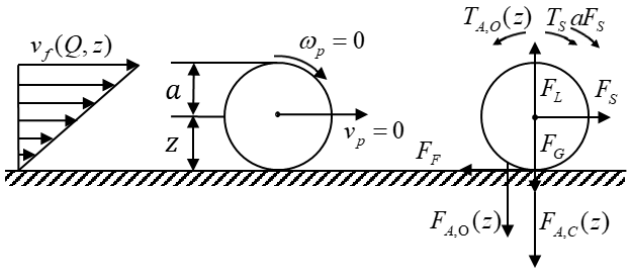

Figure 2. Model of deposited particles under shear flow.

particles upon detachment and deposition as a criterion for lateral stiffness. It was observed that although part of initially deposited particles detaches under shear flow before arrival of local dilution, detached particles could deposit again once local dilution arrives. Deposition ratio could be thus conserved up to 90% and maintain so under high shear rate (2000 s^{-1}). We conclude that dilution is play the decisive role in deposition of particles in an oppositely charged P/S system under shear flow.

2. THEORY

Our study focuses on the deposited state or the slow viscous motion of a smooth undeformable spheres with radius *a* near substrate. We assume the fluid is Newtonian fluid with viscosity μ. In order to introduce high shear rate near substrate, a flow chamber with height *h*, length *l*, width *w* was designed(see Fig. S3) and proved that can create Poiseuille flow across vertical plane along velocity direction with a controllable velocity profile $v_f(Q,z)$. While width and length of flow chamber are both over 10 times larger than height, velocity distribution along x-axis and y-axis can be neglected away from the boundaries on these two directions. With a programmed flow rate *Q(t),*

$$v_f(Q,z) = \frac{6Q}{wh^3}(hz - z^2) \tag{1}$$

$$Q(t) = 0.003125[\mathrm{mL/s^2}]\cdot t, 0s < t < 160s \tag{2}$$

where z is the elevation from substrate and t is time. Shear rate, $\dot{\gamma}$, near substrate will be constant and can be determined with the programmed flow rate as,

$$\dot{\gamma} = \frac{dv_f(Q,z)}{dz} \approx \left.\frac{6Q}{wh^2}\right|_{z \ll h} = 12.4[s^{-2}] \cdot t \tag{3}$$

When a particle is deposited as described in Fig. 2, both angular velocity ω_p and translational velocity v_p would be zero. Normal force, lateral force and torque inequality on sphere at deposited state are

$$F_L < F_G + F_{A,C}(z) + F_{A,O}(z) \tag{4}$$

$$F_S < F_F \tag{5}$$

$$T_S + aF_s < T_{A,O}(z) \tag{6}$$

where F_L is the lifting force on the particle induced by shear flow, F_G is the gravitational force, $F_{A,C}$ is adhesive force applied on contact point, $F_{A,O}$ is adhesive force applied offset from contact point, $T_{A,O}$ is torque caused by $F_{A,O}$, F_S and T_S is the drag force and torque induced by shear flow. F_F is an ensemble of possible tangential forces between particle and referred here empirically as friction force. In eqn. 4-6, detaching forces and torques are on the left of equation, while the resistant contributions are on the right. The torque balance (eqn. 6) is using contacting point as pivot and term aF_S is the torque exerted at pivot due to shear induced drag force. The lifting force[5, 38], gravitational force, shear induced force and torque[39] can be expressed as,

$$F_L(Q,z) = 6.46\mu a^2 [\frac{\rho_f}{\mu}\dot{\gamma}(Q,z)]^{\frac{1}{2}} v_f(Q,z) \tag{7}$$

$$F_G = \frac{4}{3}\pi a^3(\rho_\rho - \rho_f)\mathrm{g} \tag{8}$$

$$F_S = 6\pi\mu a z\dot{\gamma}\cdot f_{F,S}(z) \tag{9}$$

$$T_S = 4\pi\mu a^3\dot{\gamma}\cdot f_{T,\mathrm{S}}(z) \tag{10}$$

where g is acceleration due to gravity, ρ_p a1nd ρ_f are the particle and fluid density. $f_{F,S}$ and $f_{F,S}$ are correction factors extrapolated by fitting numerical result of Goldman et al.[4]

$$f_{F,S}(z) = \frac{(\frac{z}{a}) + 0.5744}{1.008(\frac{z}{a}) - 0.0826} \tag{11}$$

$$f_{T,\mathrm{S}}(z) = \frac{1.5739(\frac{z}{a})^2 - 0.6322(\frac{z}{a}) + 0.8699}{1.5753(\frac{z}{a})^2 - 0.6562(\frac{z}{a}) + 1} \tag{12}$$

At limiting case of contact ($z=a$), $f_{F,S}(z)$=1.7005 and $f_{T,S}(z)$=0.9440. When a particle is deposited, F_S is not large enough to overcome F_F, two torques induced by shear flow is no larger than $T_{A,\mathrm{O}}$ and F_L is not large enough to overcome sum of F_A and F_G. The two terms of adhesive force $F_{A,C}$ and $F_{A,O}$ add up to F_A, which is colloidal force composed of electrostatic, van der Waals, steric, depletion and bridging forces and has been previously studied.[2, 40, 41] But unlike these studies in quiescent system, under shear flow, a perfect smooth particle will have the tendency to rotate and slide. This tendency could result in slight displacement, allowing polymer bridges to stretch and induce resistance against hydrodynamic detaching force and torque. These stretched polymer bridges reside at the rear of particle and generate force having lateral component of F_F and normal component of $F_{A,O}$. $F_{A,C}$ is most similar to F_A except that $F_{A,C}$ doesn't contain the contribution of

bridging force from shear flow induced stretched polymer bridges. An schematics of polymer bridges under shear flow drawn to scale is provided in Fig. S13 to detailly illustrate the origin of F_F and $F_{A,O}$.

Upon detachment, the maximum friction force can be calculated since its value equals to value of F_S at this moment. This maximum friction force serves as a good reprehensive for lateral adhesion of a deposited particle. After detachment, particles were observed most commonly to be rolling and sliding near substrate at low shear rate. Lateral force balance and torque balance for this case follow model by Godman et al.[4](Fig. S3). At a given shear rate and elevation, all components in two balances but translational and angular velocity are known, thus v_p and ω_p can be solved. At a given elevation, velocity and angular velocity of the particle can be calculated at a given shear rate according to lateral force and torque balances(Fig. S4&S5). Normal force balance is simplified to be

$$F_L < F_G + F_A(z) \tag{13}$$

Effective bridging interaction was not observed until dilution in-situ thus F_F and $F_{A,O}$ can be neglected. $F_{A,C}$ is referred as F_A because the absence of effective $F_{A,O}$.

3. MATERIAL & METHODS

3.1. Glass Substrates.

Glass slides (Corning) were used as substrates in all experiments. Glass surfaces were sonicated in isopropanol for 30 minutes, washed with deionized water, sonicated again in 0.1 M KOH for 30 minutes, washed with deionized water and dried with high purity nitrogen.

3.2. Solutions.

To prepare the starting solution with target composition, SLES (Texapon N70, BASF) and AAC (Salcare SC60, BASF) were used as received from Firmenich, and Nominal 6.46 μm diameter silica colloids (Bangs Laboratories) were used without further purification. Four composition were tested in this study as described in table 1 and Fig. 5. Composition A is 1/60 times diluted of composition D, while composition D is a model shampoo composition. Composition B and C has the same surfactant content as composition A but increasing polymer concentration. Stock solutions of SLES and AAC in DI water were prepared separately and were sonicated until a homogenous solution is obtained. Then each stock solution of SLES and AAC was diluted in DI water to achieve concentration twice the value of target value. To mix solution, 0.5 mL AAC solution was first added to an Eppendorf tube, 0.5 mL SLES solution and 3 μL silica colloids suspension were then added separately and simultaneously to AAC solution. The tube was capped and placed forthwith on a shaker for 30 minutes to reach equilibrium.

To prepare flushing solution for a diluting experiment, authentic tap water was prepared with composition of 2.5 mM NaCl solution. The conductivity of the authentic tap water(300 μS/cm) is identical to tap water in the lab. For a non-diluting experiment, solution of SLES was added to AAC solution to prepare an AAC/SLES mixture with exact concentration with starting solution. The flushing solution did not contain silica particles. The mixture was then placed on a shaker for 30 minutes before use.

Table 1. Composition of initial formulation used in this study. Notes include: (a) AAC concentration as prepared, (b) SLES concentration as prepared and (c) figures that corresponding composition was adapted in.

Composition No.	A	B	C	D
[AAC] / wt%[a]	0.00834	0.05	0.2	0.5
[SLES] / wt%[b]	0.2	0.2	0.2	12
Adapted on figure	1,3,4A-E,5A, S1,S7,S8,S11,S14	3,5B,S7,S8,S12	3,5C,S7,S8	4F-J,5D,S9,S10

3.3. Flow cell apparatus.

Flow cell was fabricated to create a fluid chamber between two glass slides and within two blocks made with poly(dimethylsiloxane) (PDMS) (see Fig. S2 for details). The length of the flow chamber was 55 mm, the width was 5 mm, and the height was 0.55 mm. Liquid PDMS and curing agent (Sylgard 184, Dow) were mixed at ratio of 10:1 and put in vacuum to remove bubble. On each smooth surface of a 6-inch silicon wafer, 4.1 g of PDMS mixture was poured on the center. The wafer was placed on the center of a shaker and let rotate at speed of 2 rpm for 1 hour and then transferred to a convection oven with a leveled tray to cure at 70℃ for 3 h. After complete crosslinking, peel off solidified PDMS and cut out slices with a uniform thickness of 0.55 mm. The shape was cut out as described in Fig. S2B. PDMS blocks were then sonicated in isopropanol for 15 mins and in deionized water for 5 mins and dried in a vacuum oven. After exposing PDMS blocks and glass slides to oxygen plasma for 50 s before binding, blocks were placed on one glass slide symmetrically and then another glass slide was placed above to seal the flow chamber.

3.4. Experimental setup.

To connect the setup, first restrain the flow cell on a prism or under a microscope. A 50 mL syringe was used to contain around 50 mL of flushing liquid, and then connect to: female lure lock, tubing, male lure lock, 3-way stopcock and a blunt needle. Switch stopcock to stop flow to the unoccupied direction. The syringe was pushed by a syringe pump to remove air through the needle. Then the stopcock was switched to the needle and connect needle to the flow cell. Another blunt needle was connected to a tubing via a female lure lock was installed to the other end of flow cell as outlet. Epoxy was then used to fully seal the gap between needle and flow cell. Then the starting solution was transferred to a 1 mL syringe and connect a needle(B25-50, SAI). The solution was slowly injected to the flow cell by piercing through PDMS block near the entrance

of flushing fluid. To avoid air bubble, tilt flow cell while injecting so air in flow chamber could be exhausted through outlet. Pull out the needle after injection and seal the punch hole with epoxy (Loctite). Wait for epoxy to solidify and switch stopcock to unoccupied direction, then start the pump.

3.5. Microscopy & Image Analysis.

An optical microscope (Axioplan 2, Zeiss) and CCD camera was used to dynamically track and monitor colloids sedimented onto substrates. A flow cell was optically coupled to a 68° dovetail prism (Reynard Corp.) using index matching oil (n=1.515). A 10× objective was used in conjunction with a 12-bit CCD camera (ORCA-ER, Hamamatsu) at a capture rate of 28 frames/sec with 336 x 256 resolution (pixel length=607nm).

3.6. Fluid mechanics simulation.

A physics simulator (COMSOL Multiphysics 5.4 version) was used to perform fluid mechanics simulation. A time dependent, free of solute and fully developed Laminar flow with viscosity of 1 cP, density of 998 kg/m^3 were injected from inlet needle into flow chamber. Nonslip, nonpermeable boundary condition were assumed. Transport of diluted species under Laminar flow was studied. Diffusivity was assumed to be 0 because of a high Peclet number near surfaces. Normal mesh sizes with each tetrahedral mesh unit having length between 50 μm to 200 μm were adapted and boundary layers were added in setting to have a higher resolution near walls. This model was simulated to yield velocity data and concentration data from t=0 s to t=60 s with an interval of 0.2 s. These settings are applicable for composition A-C. In case of composition D, initial fluid in flow chamber has viscosity of 6 cP and local viscosity after injection of water has linear dependence with concentration.

4. RESULTS & DISCUSSION

Fig. 1 shows the experiment settings on multiple scales. On the lab scale(Fig. 1A), flow cell and accessories were build based on TIRM apparatus. The flow cell is mounted on a prism with laser aligned so that 3D trajectory of particles under shear flow can be obtained if necessary. In Fig. 1B, a close up view at the flow cell is given to help capture the real size. Red dye is added in diluting flushing fluid to signify dilution process in bulk. Fig. 1C is showing a snap from simulation near substrate when dilution arrives the first viewing window while the second viewing window further from entrance is still concentrated. The timepoint in Fig. 1C is different and postponed compared to Fig. 1B because of the difference between bulk dilution and dilution near boundary, which will be more detailly discussed in Fig. 3. After experiment, videos from microscope could be tracked as shown in Fig. 1D and will be discussed further in Fig. 4. The majority of particles can be categorized into three (Fig. 1D). In a concentrated region(e.g. the right window in Fig. 1C), detached(not heighted, grey) and constantly deposited(red) particles can be found. After dilution(e.g. the left viewing window), redeposited particles (blue) and constantly deposited particles can be observed. Molecule scale schematics for P/S configuration in Fig. 1E illustrate the mechanism for deposition and detachment. The dependence of configuration on dilution and formulation will be discussed in Fig. 5.

4.1. Dilution process

As mentioned earlier in this paper, dilution is found to have a close connection with deposition behavior of particles. Before explaining this connection, dilution and shear rate profile will be discussed to help better understand dilution process. In Fig. 3, a simpler case without

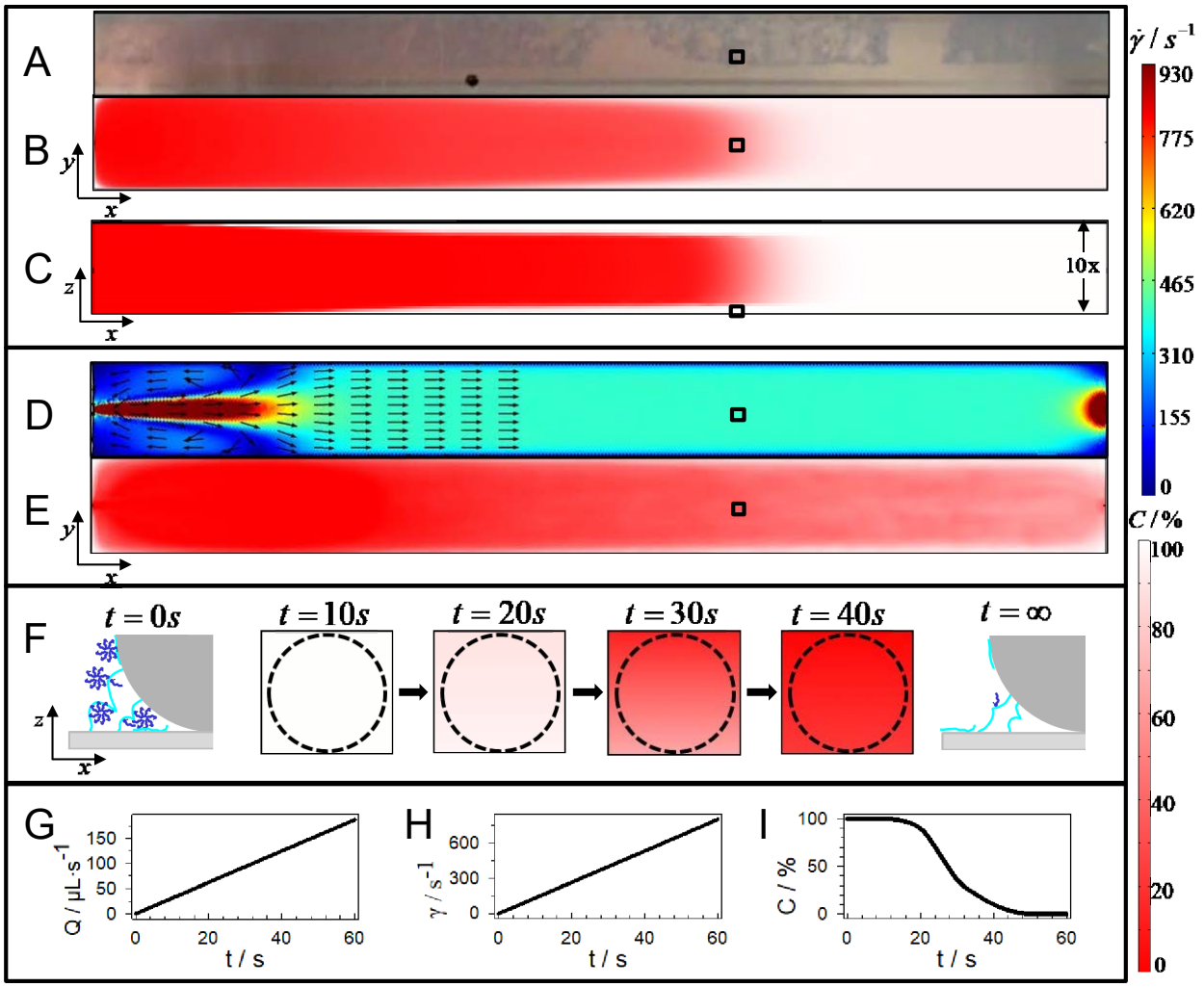

Figure 3. Dilution and shear rate profile in flow cell. Simulation result is applicable for diluting experiments starting with composition A,B&C. **(A)** A top view of experiment when dyed flushing liquid arrives at viewing window(t=7.8s). Viewing window 3.5 cm from entrance is marked as black squares. **(B)** A top view of dilution profile averaged over thickness when averaged dilution arrives viewing window(t=6.8s). **(C)** A side view of dilution profile when averaged dilution arrives viewing window(t=6.8s). The snap is magnified along z-axis by 10 times for clear view. **(D)** Shear rate profile near substrate (z=a) on local dilution (t=30s). Normalized arrows show direction of fluid velocity. **(E)** Dilution profile near substrate (z=a) on local dilution (t=30s). **(F)** Snaps of dilution process around a deposited particle on side view. **(G)** Flow rate profile from pump programing. **(H)** Shear rate profile at z=a. **(I)** Dilution profile at z=a.

viscosity change after dilution is discussed. This is applicable to composition A-C. Composition D is more concentrated and the effect of viscosity change on dilution is discussed in SI.

Figure 3A-C show dilution bulk solution. In simulation, concentration along z direction was averaged up and shown in Fig. 3B as a direct comparison with color change in experiment. Time before color change in experiment (7.8s) is comparable to that in simulation (6.8s). Since air

is inevitable as barrier between the changing composition and the compliance of plastic syringe is inevitable, this deviation is within tolerance. Considering that flow rate at the beginning is extremely slow but ramping (Fig. 3G,3H), deviation between experiment and simulation should subside to a negligible value over time. Side views along(Fig. 3C) and view normal(Fig. S8D) to flow direction are also shown at timepoint when dilution in bulk arrived. It can be shown in Fig. 3C that dilution away from boundaries are uniform along z direction while dilution near substrate is much slower and dependent on elevation. A much slower fluid velocity near boundaries compared to that in bulk is accountable for this phenomenon. Convection near boundaries will thus be slowed.

Figure 3D-E show shear rate profile and concentration profile at one particle radius above substrate at timepoint when dilution arrives in viewing window. Vortexes can be observed near entrance but not the exit. The entrance effect could result in much higher shear rate in the unequilibrated region that could easily detach particles. Detached particles are likely to be either trapped in vortexes or lifted into bulk and detach rapidly. Viewing windows for data acquisition are chosen away from entrance to avoid unequilibrated flow.

Figure 3F shows a side view of dilution process around a deposited particle. Before(t=0s) and after(t=∞) dilution, the schematics starting with composition A as representative show mechanism of deposition and preferential dilution in adsorbed layer. Simulated concentration profile helps reveal the dilution process in between. On this micrometer scale, the boundary of dilution behaves like approaching toward substrate. Simulation shows in situ dilution begins at t=18s and ends at t=45s (Fig. 3I). This process takes a long time because of slow velocity near substrate and also because diffusion coefficient was assumed to be zero. Diffusion coefficient of surfactant will be reduced with the formation of micelles and be further decreased if in neutral

polymer solution, where the value would be on the magnitude of 10^{-8} cm^2/s.[42] Considering the opposite charge on P/S in this study, the diffusion coefficient could be lower. Peclet number for surfactant in such system is at least two order of magnitude greater than 1. To decrease unnecessary complexity, diffusion is neglected in our simulation.

Dilution is postponed in the case of composition D. It takes 52 s to reach 50% dilution near substrate with viscosity change (Fig. S9J), 24 s longer than case without change in viscosity (Fig. 3I). This difference can be explained by Saffman-Taylor instability or "viscous fingering", in which high viscosity fluid can will be displaced by injected low viscosity fluid for higher mobility and Péclet number.[43] Slower movement near substrate relative to the bulk result in slower dilution on surface, which subsequently leads to high viscosity fluid staying longer, and in turn more resistance promotes slower dilution. Simulation result with composition D is included and discussed in Fig. S8 and S9.

4.2. Deposition behavior vs. dilution

Raw data is illustrated and correlated with time. The experiment and simulation were performed starting with composition A&D, diluting flushing liquid was used, and video was taken 3.5 cm from entrance. With our tracking algorism, deposited particles were tracked and categorized into constantly deposited and redeposited particles (Fig. S10). The number of deposited particles from different sources were counted as a function of time in Fig. 4A&F. The curves could be divided into three stages. The first detachment stage starts with the application of flow and ends with the surge in redeposition. During this stage, portion of initially deposited particles would detach with increasing shear rate and be washed off with flow. The second redeposition stage lasts few seconds during the surge of redeposition curve. A large portion of detached particles in view redeposited and fewer detached particles from upstream were observed

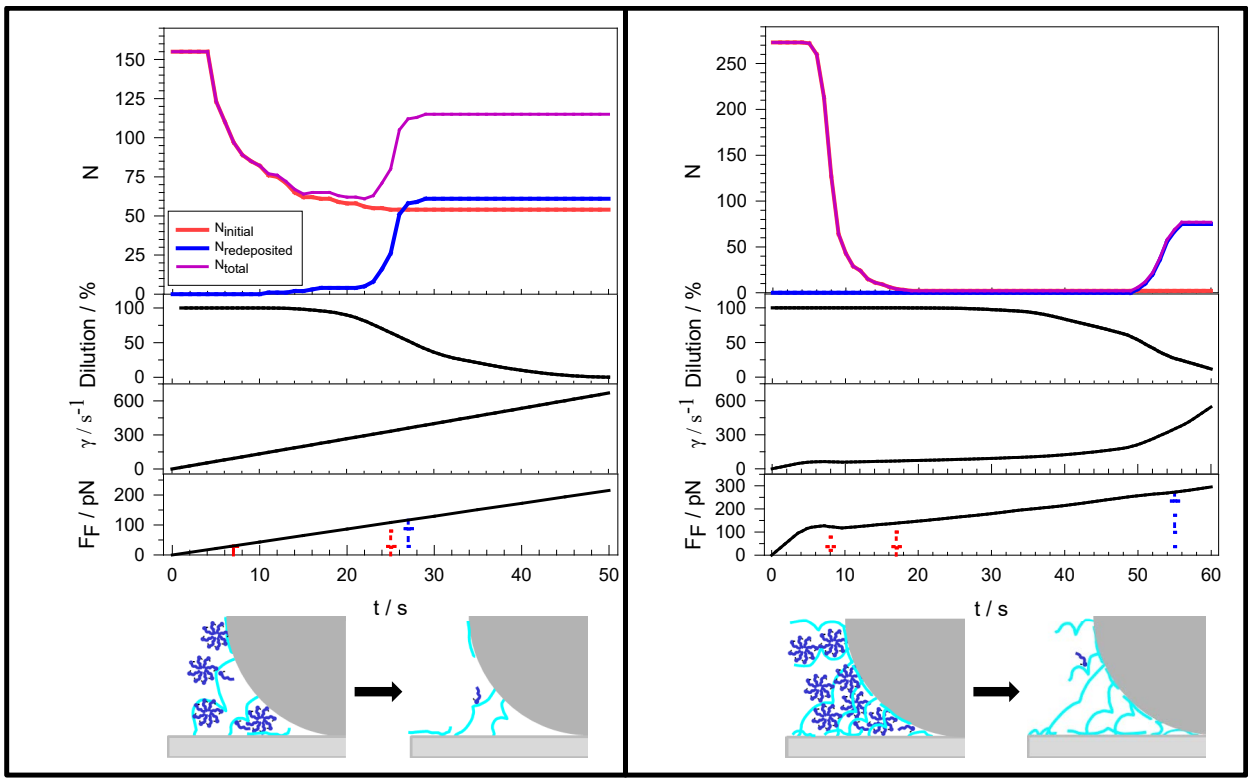

Figure 4. Deposition count from experiment and modeling data. (A-E) Data for composition A. **(F-J)** Data for composition D. **(A,F)** Count of deposition particle. Red line shows number of particles constantly deposited since the initial frame, blue line shows number of redeposited particles, purple line shows total number of deposited particles. **(B,G)** Dilution profile at z=a. **(C,H)** Shear rate profile at z=a. **(D,I)** Friction force change on detachment and deposition. Red arrow indicates change of friction force upon average(left) and last(right) detachment, blue arrow indicates average change upon deposition. **(E,J)** Schematics for two composition before and after dilution.

as redeposition stage proceeded. Finally, all curves plateaus and no further detachment of either constantly deposited particles or redeposited particles was observed. In this stiffly deposited stage, redeposition is still possible but was not observed because there are no detached particles from upstream. The stiffly deposited stage lasted until the end of experiment, where shear rate kept ramping up to 2000 s^{-1} and the particles stayed deposited.

In comparison, as soon as dilution profile in Fig. 4B&G indicates the ongoing of dilution in solution near substrate, behavior of particles proceeds from detachment stage to redeposition stage. This revealed the strong connection between deposition and dilution in fluid near substrate. More experiments were done by adjusting the distance of viewing window from entrance, so that

dilution could be postponed further away from entrance. Results show that by postponing dilution, the redeposition stage is also postponed with good consistence in their timepoints. Redeposition was not observed in experiments using nondiluting flushing fluid (Fig. S11&S12). Thus, it is concluded based on these observations that in situ dilution in fluid results in redeposition of detached particles.

The detaching force applied on a detached particle is higher when they redeposit than when they detached. Based on hydrodynamic analysis discussed in theory part, friction force(Fig. 4C&H) upon detachment and redeposition can be calculated depending on shear rate(Fig. 4D&I). Red arrows marked the averaged (left) and last (right) friction force at detachment. In Fig. 4I with composition D, initial hydrodynamic detaching forces and torques are 6 times higher than in Fig.4D given the same shear rate because of higher viscosity. A large detaching force in this case at the beginning may be one of the reasons for severe detachment. It is interesting that redeposited particles in both cases overcame higher detaching force (equals to friction force) to redeposit than when they detached. This indicates, very likely, a composition change in adsorbed layers on particles and substrate, which result in a different deposition mechanism as illustrated in Fig. 4E&J.

Friction force analysis provides a good measurement for lateral stiffness of deposited particles. For both experiments in Fig. A&F, a great portion of initially deposited particles detached right after the start of flow (the drop at the beginning has a delay from t=0 because of compliance in the pumping system and a tolerance in tracking code before categorized as detached). Effective lateral adhesion able to provide resistance against shear may not even present for these particles. Deposition of such particles could be a result of pure normal adhesion in quiescent condition. While our previous work using TIRM to accurately measure such normal

stiffness of deposition, friction force analysis could provide extra data on their lateral stiffness.

4.3. Preferential dilution

Before local dilution, deposition of particles is weak and vulnerable to shear flow. After dilution, particles are strongly deposited and can resist high shear rate. This change in lateral adhesion is mostly likely a result of change in composition of adsorbed layer, which is inevitably associated with dilution in fluid near substrate.

While dilution in fluid has no preference on solute, possible ways for dilution on adsorbed layers can be categorized into four: negligible dilution of both P/S, significant dilution of both P/S, preferential dilution of polymer and preferential dilution of surfactant. In the case of negligible dilution of both P/S, a significant difference in lateral adhesion between pre-dilution and post-dilution should not be observed. In the case of significant dilution of both P/S, particle could not deposit after dilution according to the state diagram (Fig. 5E). Composition of adsorbed layer could be diluted into green region, in which particles would not deposit even without flow. Preferential dilution of polymer is not likely to happen. Surfactant does not have direct attraction with substrate but strong electrostatic repulsion. Without adsorbed polymer, surfactant cannot resist shear flow and stay near substrate.

Preferential dilution of surfactant is the most possible scenario. As reported, shear flow could distort polymer chains in a P/S system and enhance exchange of surfactant in absence of dilution.[23, 25] If dilution is coupled with shear flow, such exchange of surfactant could very likely lead to dissociation from adsorbed layer into fluid because of a much lower concentration. Adsorption of cationic polymer on substrate can be easily maintained under shear flow with aid of electrostatic attraction.[21] Such preferential dilution behavior has been reported before by Biggs et al.[28] and Dedinaite et al.[29]. According to our steady state study, in the absence of surfactant a little

amount of polymer is sufficient to deposit particles. We surmise that during dilution in local fluid, preferential dilution of surfactant happens on the adsorbed layer while polymer stays adsorbed and regains more free positive charges.

It is worth noticing that adsorbed layer on detached particles could also be preferentially diluted. Detached particles have translational movement with velocity around half of fluid velocity. So detached particles could be immersed in diluted liquid even though they are both transiting in the same direction. The velocity difference together with rotation of particles ensures shear around the detached particles, thus adsorbed layer on detached particles can also be preferentially diluted in a similar way as on substrate.

4.4. Deposition behavior vs. starting composition

It has been studied in our previous work that normal deposition behaviors of particles are varying with different P/S composition[17]. Above a critical P/S concentration, particles would be all normally deposited with no little difference. However, such normally deposited particles could have different lateral adhesion behaviors under the impact of shear flow. In application of complex fluid, such as daily care product, it is difficult to alter fluid dynamics environment. To increase percent deposition, the easiest way is to develop a formulation most favorable to deposition under representative fluid dynamics environment. Deposition behaviors of particles immersed in different diluting P/S composition were summarized in Fig. 5. Key steps, including deposition before introduction of flow, detachment under shear, redeposition on dilution and a final stiffly adhered state, were marked on deposition profile and illustrated with schemes. By understanding mechanism behind detachment and deposition behaviors, better formulation could be developed to optimize percent deposition.

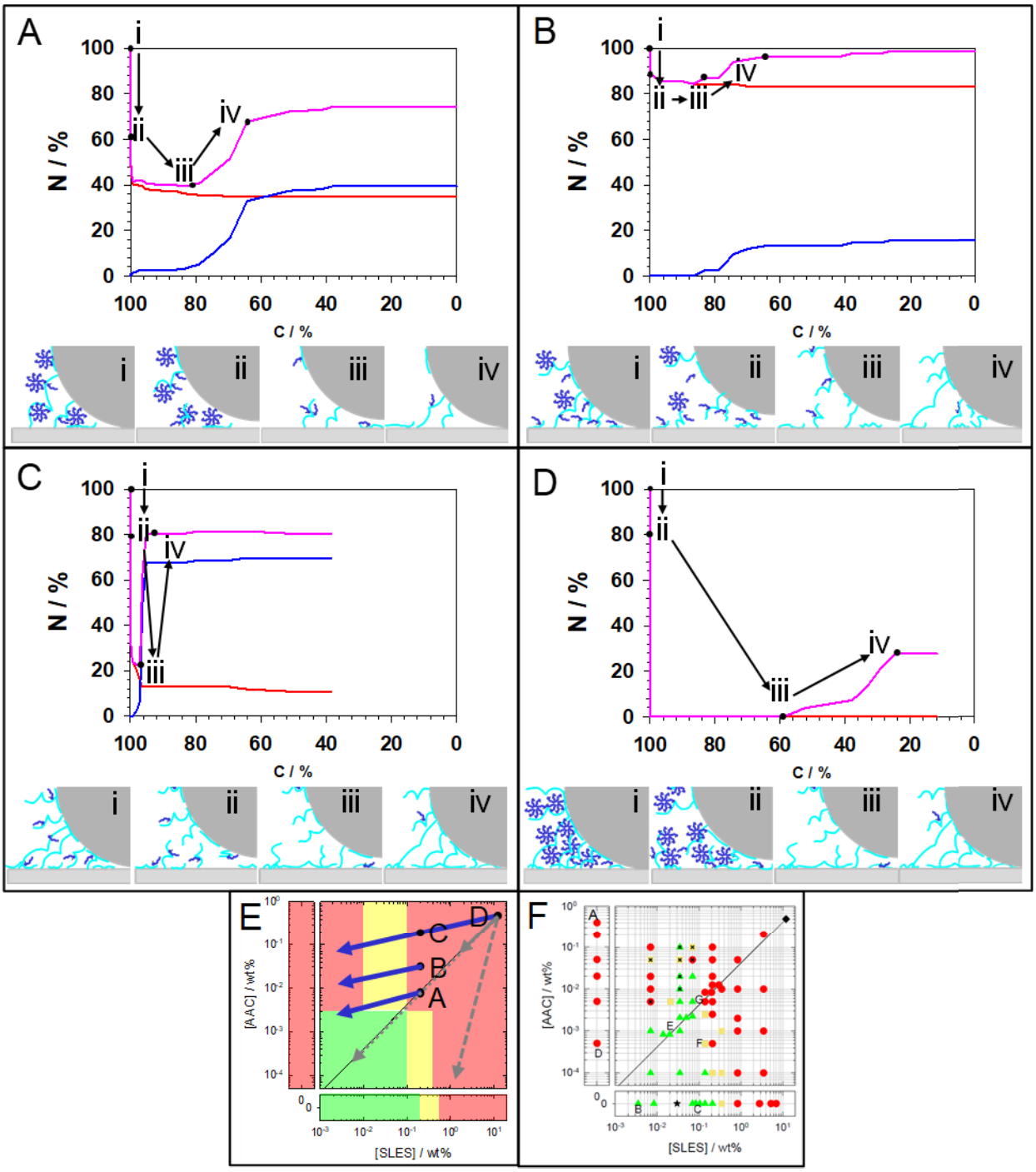

Figure 5. Deposition ratio in relation with dilution change and schematics at key steps during dilution. Plots in **A-D** show dependence of deposition behavior, including initially deposited(red), redeposited(blue) and total deposited(purple), on dilution process. Schematics (not to scale, size of molecules are extravagated) below describe P/S configuration and deposited/detached status at key steps corresponding to deposition profile. **(E)** A state diagram noting starting composition in A-D summarized based on our previous work **(F)**[17].

In Fig. 5A, where the solution starts with composition A, 65% of particles detached before dilution. While 62% of detached particles redeposited, a final percent deposition of 74% were

obtained. Because of a low polymer/surfactant ratio in composition A, there are not enough positive charges to bind surfactant molecules. Micelles present widely around positively charged sites on polymer chains that weaken bridging interaction between particle and substrate. Particles detach easily moving from step i to step ii. As is concluded in the last section, dilution in solution near substrate result in a preferential dilution of surfactant in adsorbed layers. At step iii, surfactant molecules on both adsorbed layers are preferential diluted. Positively charged sites on polymer chains were exposed. Once a detached particle contacts substrate, polymer bridges would form and bring particle into the transitional stage(Fig. S4A). Particles will be slowed down, and more bridges will form between adsorbed polymer layers and vacant sites on both surfaces. A particle will thus be stiffly deposited as illustrated in step iv. In the experiment, shear rate keeps ramping up to $2000s^{-1}$ and these deposited particle stays adhered.

In Fig. 5B, composition B was tested. At the same surfactant concentration, stronger lateral adhesion before dilution was observed with additional polymer. Only 17% of particles detached and 92% of detached particles redeposited after dilution, resulting in a high final percent deposition of 99%. Compared to Fig. 5A, higher polymer/surfactant ratio decreased concentration of micelles in solution and adsorbed layers by binding more surfactant onto polymer. More positively charged sites were exposed on polymer thus resulting in stiffer binding. The polymer concentration is also not too high that there are enough vacant sites on surfaces for polymer bridges to anchor. In Fig. 5C, where concentration of polymer in composition C is further increased, overall charge is almost neutral in PS composition. Higher cationic exposure did not bring stiffer adhesion. With 88% of initially deposited particles detached and 79% of them captured on dilution, final percent deposition of 80% was obtained. Lateral stiffness before dilution shows non-monotonic dependence on polymer concentration. Lack of vacant sites on both surfaces could be the one of

the reasons for such reversed trend. Polymer chains with further increased concentration also have higher density of unoccupied cations and are crowded on surfaces. Severe detachment before dilution could be a result of the lack in anchoring sites on each polymer bridges. The lack of surfactant on each polymer chains may also bring about this weak lateral stiffness. Composition C is close to the coacervation region, where PS complexes are overall neutral and coacervation forms. The decrease in solubility may also be unfavorable the formation of bridges. After dilution, as surfactant molecules are washed off, solubility will be restored.

Figure 5D is using composition D. This formulation contains large amount of both polymer and surfactant. Coacervation formed in some of our studies depending on mixing procedure that could interfere repeatability. Coacervation was not observed in result reported here, the solution was clear and uniformly viscous. Overall polymer/surfactant ratio for this composition is the same as composition A. Before dilution, polymer chains are suspected to be saturated with surfactant and bridging interaction is weak. Once shear flow is applied, all particles detached soon(also see Fig. 4F). A final percent deposition of 30% was obtained. The presence of viscosity difference slows dilution near substrate and gave detached particle more time to be washed off. Unlike deposition stage in experiment with low concentration, it is observed that deposition stage of detached particles lasted longer. Since the first deposition of a detached particle, other detached particles could still translate across window. Detached particles were not simultaneously deposited in this stage. Also, while most particles deposit singularly on substrate with composition A,B&C, a considerable portion of particles deposited on dilution were captured by deposited particles rather than substrate. The provided final capture ratio could be underestimated since it is challenging to accurately count number of particles in aggregates. These phenomena indicated quite different deposition process with high PS concentration. Substrate could have been saturated by polymer

chains that vacant sites are insufficient for detached particles anchor to. As all initially deposited particles detached on shear flow, 30% of them were captured after dilution.

Composition could affect deposition at least through 2 major ways, polymer/surfactant ratio and polymer concentration. A larger polymer/surfactant ratio could favor lateral stiffness under low polymer concentration. Higher available cation ratio on polymer chains provides polymer bridges with more anchors and thus strengthen bridging interaction. High polymer concentration is unfavorable to lateral stiffness that high adsorbed density may result in insufficient anchoring sites on surfaces. Although deposition of detached particle could help increase final percent deposition, gravity may not be in favor of maintaining detached particles near substrate in application. Substrates are often parallel to gravity in applications such as rinsing shampoo from hair. Under such circumstance, detached particles few hundred nanometers away from substrate will be constantly lifted away and be washed off rapidly. To best increase final percent deposition, the best way could be avoiding detachment in the first place. Further research will be focused on more sophisticated designs of particle shapes to minimize detachment.

5. SUMMARY & CONCLUSIONS

Deposition behavior of colloidal particles in PS solution under diluting shear flow was measured and related to local dilution profile. Without dilution, the deposited particles detach with increasing shear rate. After dilution in fluid near substrate, large portion of laterally detached particles could deposit again, and deposited particles remain stiffly adhered on substrate. By varying initial composition, different detachment behavior and final percent deposition was observed. These findings revealed the important role of dilution and composition in depositing colloidal particles in a system with polymer and surfactant.

Consistent with our previous work,[17] particles are deposited in quiescent fluid under conditions tested. When particles are deposited by strong normal adhesion, methods such as TIRM show little difference with different compositions. However, shear (tangential force) could detach normally deposited particles and induce different lateral detachment behaviors with different compositions. Critical tangential force could be calculated from shear rate on detachment as a criterion for lateral stiffness. The combination of preferential dilution and initial composition determines final percent deposition. Preferential dilution of surfactant on adsorbed layer exposes positive charges on polymer and enables redeposition of detached particles. Percent deposition could be maximized if detachment is minimized. Strong lateral stiffness before dilution inhibits detachment and can be optimized by adjusting composition. At a constant surfactant concentration, lateral stiffness increases with polymer concentration at lower region and decrease at higher value. This research provides an illustrative mechanism for particle deposition under nonequilibrium dilution of P/S composition. These findings could help design better formulation for a higher colloidal deposition efficiency and be inspiring to application such as personal care product.

In future work, other factors such as roughness of particles or mixing order of P/S with colloids will be investigated. Roughness or novel shapes of particles could not only convert normal adhesion to lateral stiffness, the increased surface area close to substrate could be favorable to stiffer adhesion. Addition order in mixing colloids with P/S, which can be simply adjusted based on current manufacturing protocol, could also significantly affect strength of adhesion according our latest research.

6. APPENDIX

6.1. Microscopy Apparatus

To create a fluid condition best resemble the situation of washing shampoo off hair and to create a uniform linear shear flow dependent only on elevation, a flow cell was designed to accommodate flow with shear rate up to 2000 s^{-1}. This maximum shear rate is estimated based on a model of falling liquid film on sphere by Wild et al.[44] and the maximum flow rate (2.5GPM) suggested by Energy Policy Act. Such a model is a good estimation of shear flow falling on sphere without modification. In the presence of hair, shear rate should be lower than this estimated value because of higher hindrance from a structured porous structure. Figure S1.A is an illustration of connection and position for sample injection.

To help compare deposition behavior before flow with our previous study and examine the change after dilution, flow cell is mounted on an apparatus for Total Internal Reflection Microscopy (Figure S1B). Instead of sealing fluid with an o-ring and a cover slide, two PDMS blocks with designed shape (Figure S2) and another glass slide were adhered on the bottom slide. Laser was aligned that the beam hits one side of glass prism vertically. The laser was turned off during the flow to avoid disturbance to video.

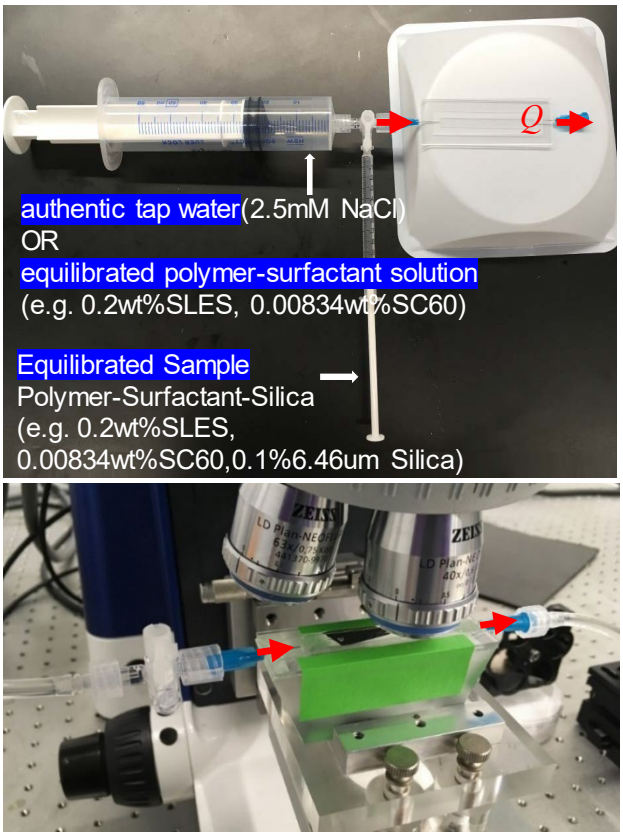

Figure S 1. Installment and setup of flow cell apparatus. (A) Illustration of a fabricated flow cell, starting fluid and flushing fluid are injected. **(B)** The microscope and the flow cell apparatus are mounted on the air table before experiment, and the flow cell is fixed on a prism. Diluting or nondiluting flushing fluid is injected from left and pushes through initial polymer/surfactant/colloid solution.

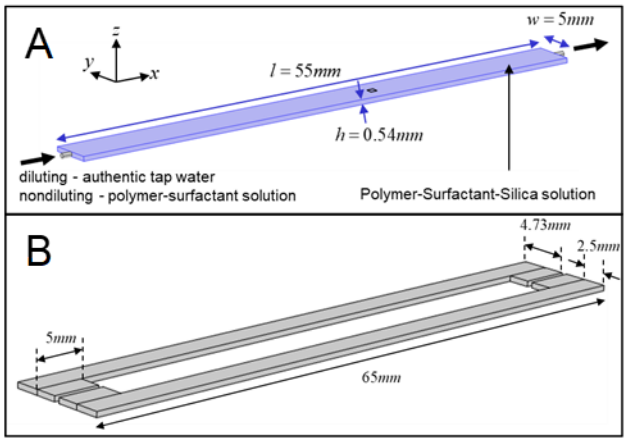

Figure S 2. Design of flow cell apparatus. (A) The dimensions of the flow chamber are described. A black square on the Fig. denotes the position 3.5 cm from the entrance where most videos were shot. **(B)** The dimensions of two identical PDMS block are described. A separation with width of 0.54 mm was left between two blocks for insertion of blunt needles.

6.2. Hydrodynamics for detached particles

A detached particle is most often observed to be rolling and sliding near substrate. Translational velocity can be recorded by tracking motion of each particle. While rotation of perfectly isotropic spheres is hard to track, it is observed on some of slightly deformed particles together with majority of perfect spheres. Such slow viscous motion of sphere near substrate has been studied by Goldman et al.[4] In Fig. S3 when shear rate is not high enough to overcome adhesion and gravity, assumption that $z \approx a$ is made. Also, while focus of microscope was fixed at particle center, detached particles were still in focus while rolling away. In sample calculation, z/a was taken as 1.0032. This is the largest value applicable in asymptotic lubrication theory by Goldman et al. Reasons for not strictly contact (z/a=1) were given by Goldman et al. including effects of surface roughness, infinite velocity gradient approaching contact, inertial effects etc. In our experiment, polymer adsorbed on substrate and particle could also act like buffer with thickness of few nanometer between two hard surfaces.

While colloidal force may still exist between a detached particle and substrate, it is highly dependent on separation and suspected to be small. Gravity and hydrodynamic lifting force should be dominating in normal direction. Equation for normal force nonequilibrium will be the same as

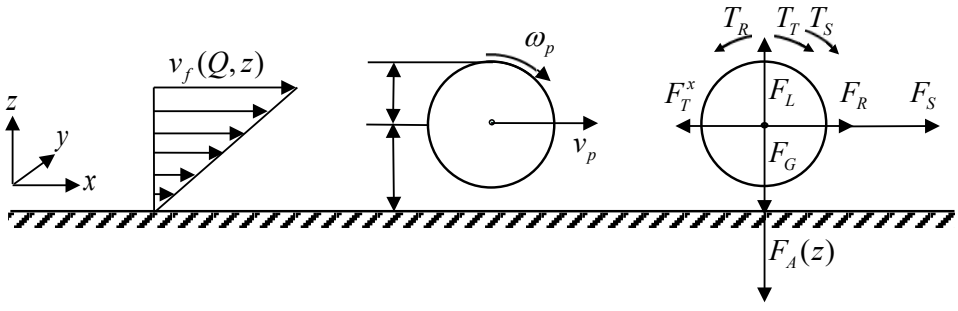

Figure S 3. Model of a detached particle under shear flow.

described in deposited state. With rotational movement and translational movement, each could contribute to pressure tensor on sphere surface. The lateral forces and torques about mass center were integrated expressed in simple format by Goldman et al. The lateral force balance becomes,

$$F_R + F_S = F_T^x \tag{14}$$

where F_T^x is drag force induced by translational movement in x direction and F_R is drag force induced by rotational movement,

$$F_T^x(Q,z) = 6\pi\mu a v_p \cdot f_{F,T}(z) \tag{15}$$

$$F_R(Q,z) = 6\pi\mu a^2 \omega_p \cdot f_{F,R}(z) \tag{16}$$

$$f_{F,T}(z) = \frac{8}{15}\ln(\frac{z}{a}\text{-}1)\text{-}0.9588 \tag{17}$$

$$f_{F,R}(z) = -\frac{2}{15}\ln(\frac{z}{a}-1)-0.2526 \tag{18}$$

At contact, z/a = 1.0032 and two factors have value as $f_{F,T}(z)$=-4.02 and $f_{F,R}(z)$=0.51. The torque balance for a detached particle is,

$$T_R = T_T + T_S \tag{19}$$

where T_T is torque induced by translational movement in x direction, T_R is torque induced by rotational movement,

$$T_T = 8\pi\mu a^2 v_p \cdot f_{T,T}(z) \tag{20}$$

$$T_R = 8\pi\mu a^3 \omega_p \cdot f_{T,\mathrm{R}}(z) \tag{21}$$

$$f_{T,T}(z) = -\frac{1}{10}\ln(\frac{z}{a}-1)-0.1895 \tag{22}$$

$$f_{T,\mathrm{R}}(z) = \frac{2}{5}\ln(\frac{z}{a} - 1) - 0.3817 \tag{23}$$

At contact, z/a = 1.0032 and two factors have value as $f_{T,T}(z)$=0.385 and $f_{T,R}(z)$=-2.68. By solving lateral force balance and torque balance at a given height with known shear rate, the value of v_p and ω_p can be calculated as,

$$v_p(Q,z) \sim v_f(Q,z) f_{L,v}(z) \tag{24}$$

$$\omega_p(Q,z) \sim v_p(Q,z) f_{L,\omega}(z) \tag{25}$$

$$f_{L,v}(z) = \frac{0.7431}{0.6376 - 0.200\ln(\frac{z}{a} - 1)} \tag{26}$$

$$f_{L,\omega}(z) = 0.5676 z^{-1} \tag{27}$$

At contact, z/a = 1.0032 and two factors have value as $f_{L,v}(z)$=0.4529 and $f_{L,\omega}(z)$=0.5315a^{-1}.

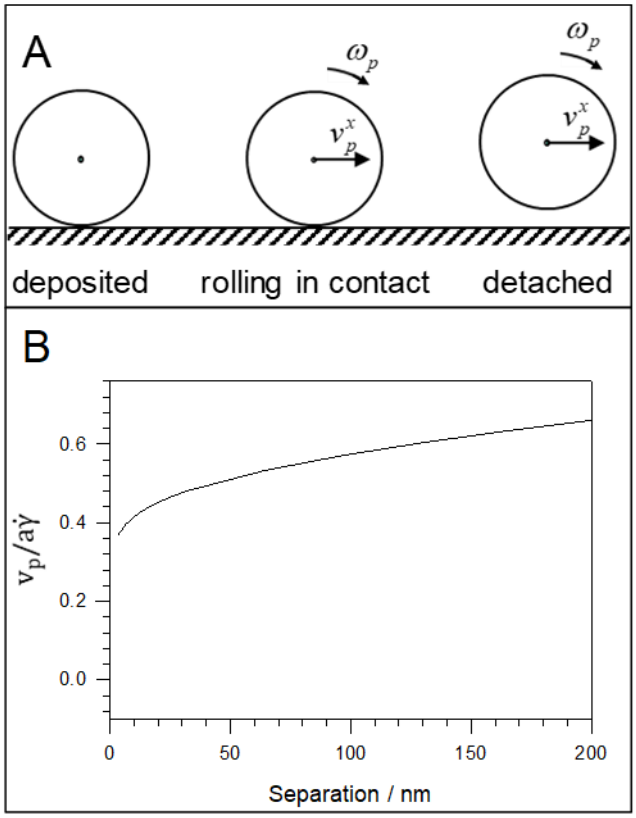

Figure S 4. States of particle and velocity profile in relative to elevation. (A) Three states of particle motion, deposited(left), rolling in contact(middle) and detached(right). **(B)** Relation between the ratio of particle velocity to the fluid velocity at the height of a particle radius with separation between surfaces.

Three commonly observed states of particles under shear flow are described in Fig. S4A. In the process of detachment, a deposited particle will start to roll while remaining in contact with substrate. Such rolling in contact state is transitional in our study before the particle would be elevated to a detached state. While particles are detached, it is likely that they would be further lifted far from substrate if shear rate is high enough. In this situation, velocity of fluid could be up to 40 times higher than near substrate, and ratio between particle velocity and fluid velocity will be asymptotic to 1. Fast washing off of such particles can be observed with particles out of focus translating rapidly across window. Since they cannot be captured by substrate and cannot contribute to percent deposition, this state is not studied in this paper. During deposition of a detached particle, it will contact surface and enters the “rolling in contact” state and then be

captured by lateral adhesion and deposit. Similar categorization has also been used in other reports.[45]

While colloidal forces are sensitive to height within few tens of nanometer, rolling particles in contact with substrate are usually reported to be moving much slower than fluid because of such interactions. As will be discussed in section III, detached particles are observed to be moving with a velocity comparable to fluid velocity and agrees with model in which colloidal forces is not included. Therefore, detached particles are speculated to have separation of tens to few hundreds nanometer from substrate and experiencing negligible colloidal forces compared to hydrodynamic forces. With such separation, particles could still be within focus under microscope. The precise separation is hard to measure with hydrodynamic method. Figure S4B shows monotonic relationship between particle/flow velocity ratio to separation. But this dependence is not sensitive enough within such magnitude. It is not reliable enough to back calculate the separation with tracked particle velocity. However, the precise separation is not critical to the current research and hydrodynamic analysis is good enough for an order of magnitude estimation. The precise value could be measured by TIRM with our current flow cell apparatus. Similar research has also been conducted combining TIRM with flow devices.[46]

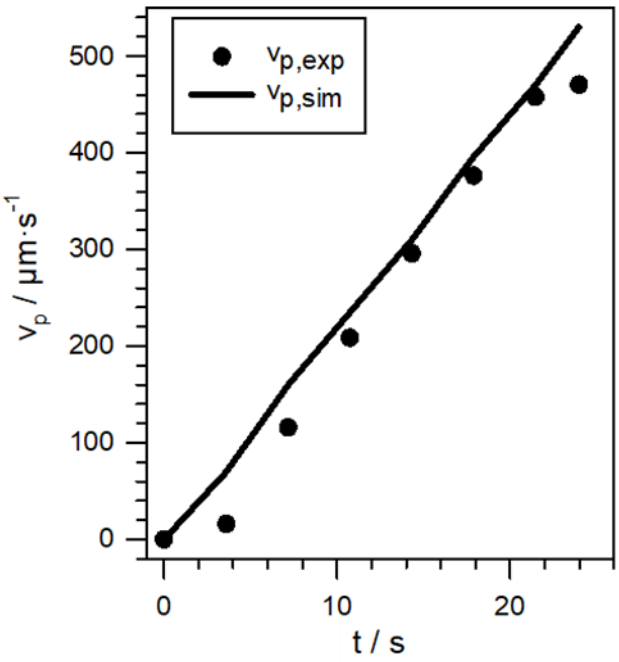

Figure S 5. comparison of particle velocity from experiment and simulation.

6.3. Particle tracking velocimetry

As discussed in the previous section, the force and torque balance include four variables, translational velocity, angular velocity, shear rate and elevation. By assuming contact and with given shear rate, translational and angular velocity of a detached particle could be calculated. Thus, velocity of tracked particles could be compared with velocity predicted this model. Figure S5 shows good agreement between experiment and simulation in an experiment without viscosity change. The experiment start using composition A (0.00834wt% AAC and 0.2wt% SLES), diluting shear flow was applied, and video was taken 3.5 cm from inlet. Comparison ends after 25 s because all moving particles deposited on substrate.

6.4. Simulation of dilution and shear rate

In order to prove reliability of our simulated fluid mechanics result, food dye was added to flushing solution to indicate concentration change in bulk solution. Time before color change in viewing window is compared with dilution time from simulation. Under condition without viscosity change (Fig. S6A&B), it took 7.8 s before red dye reaching viewing window. Compared to 6.8s required by simulation, the error is within tolerance. In Fig. S8A&B , red dye reached viewing window 6.6s after it entered flow cell compared to 6.3s by simulation. To be noticed, red dye entered flow cell 7 seconds after pump was started. This interval could be a result of air at front of needle or deformation of piston. Low volumetric velocity at the beginning of pumping profile exacerbated this lag.

Dilution near substrate under presence of viscosity change is much slower than in the absence. This can be seen by comparing Fig. S7 and Fig. S9, although dilution in bulk takes similar amount of time, it is much slower near substrate with viscosity change(Fig. S6&Fig. S8). It takes 27 s to reach 50% dilution near substrate without viscosity change(Fig. S7), but 52 s for the case with change in viscosity (Fig. S9). Shear rate profile in Fig. S7I shows good linearity increasing with time. With disturbance of viscosity change proportionally with time at the beginning. After dilution in the bulk comes through the chamber and arrives the exit , slow dilution together with slower shear rate is predicted near substrate. After dilution near substrate, shear rate increases swiftly and will be asymptotic to the result at constant viscosity. These differences can be explained by Saffman-Taylor instability or “viscous fingering”, in which high viscosity fluid can will be displaced by injected low viscosity fluid for higher mobility and Péclet number.[43] Slower movement near substrate relative to the bulk result in slower dilution on surface, which subsequently leads to high viscosity staying longer, and in turn more resistance promotes slower

dilution.

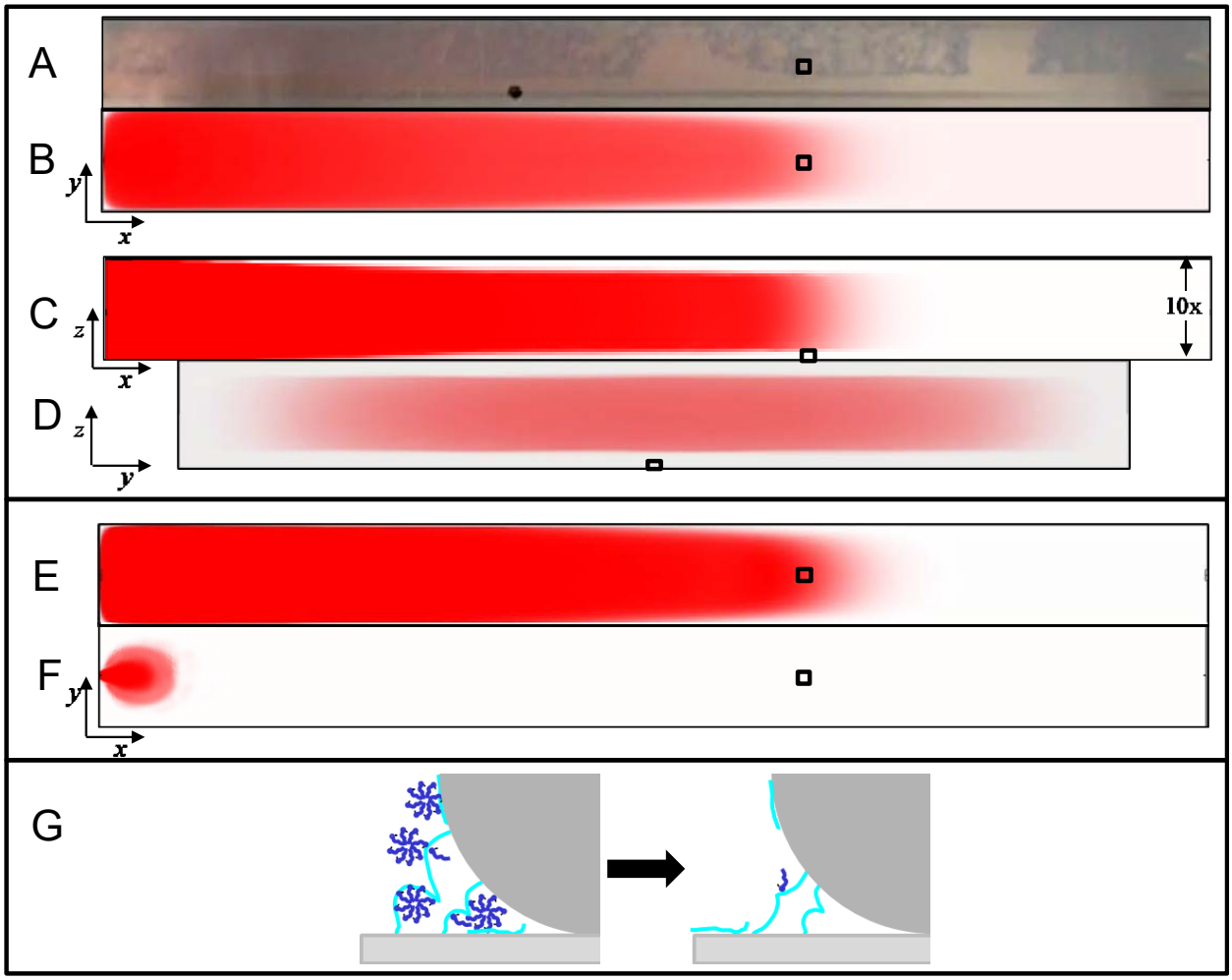

Figure S 6. Dilution profile in flow cell for composition A, B, C. (A) A top view of experiment when dyed flushing liquid arrives at viewing window(t=7.8s). Viewing window 3.5 cm from entrance is marked as black squares. (B) A top view of dilution profile averaged over thickness when averaged dilution arrives viewing window(t=6.8s). (C) A side view of dilution profile when t=6.8s. The snap is magnified along z-axis by 10 times for clear view. (D) A cross section view of dilution profile normal to flow direction when t=6.8s.(E) Top view of dilution profile of a layer at the center(z=h/2) of flow chamber when t=6.8s. (F) Top view of dilution profile of a layer one particle radius from substrate (z=a) when t=6.8s.(G) A schematics showing change in adsorbed layer before and after dilution.

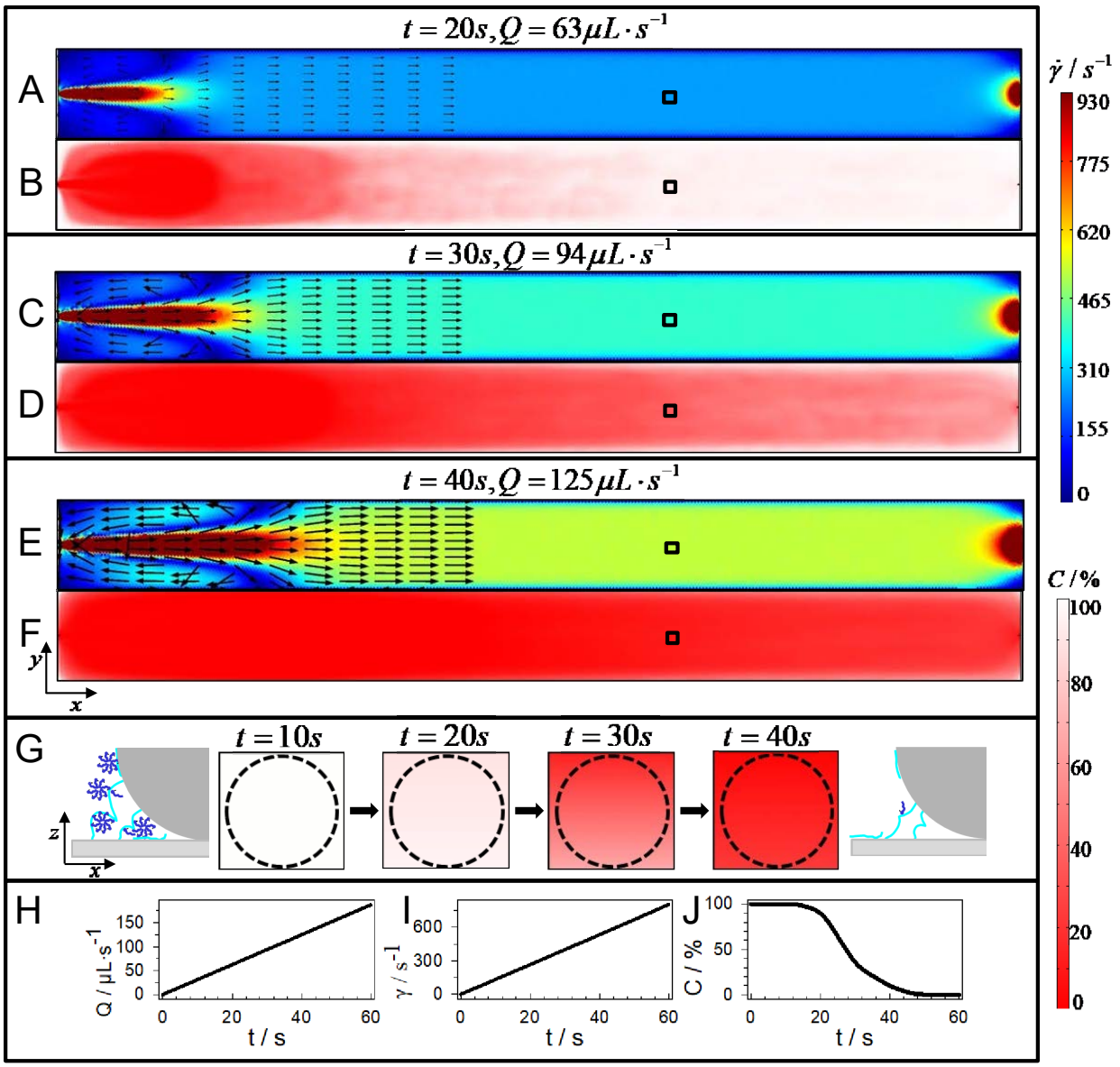

Figure S 7. Dilution and shear rate profile in flow cell for composition A, B, C. (A,C,E) Shear rate profile near substrate (z=a) at different time point. Normalized arrows show direction of fluid velocity. **(B,D,F)** Dilution profile near substrate (z=a) at different time point. **(G)** Snaps of dilution process around a deposited particle on side view. **(H)** Flow rate profile from pump programing. **(I)** Shear rate profile at z=a. **(J)** Dilution profile at z=a.

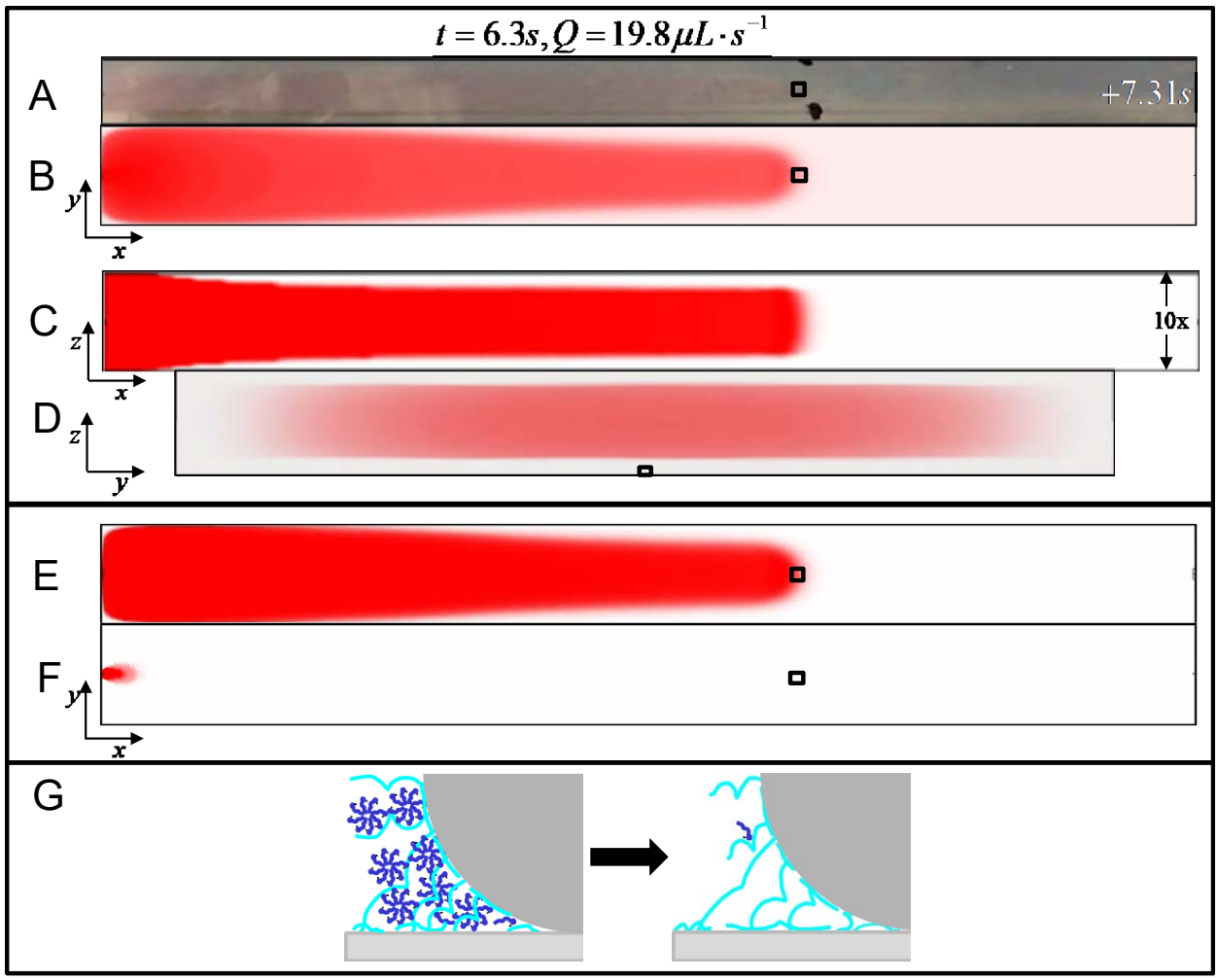

Figure S 8. Dilution profile in flow cell for composition D. (A) A top view of experiment when dyed flushing liquid arrives at viewing window(t=13.6s). Viewing window 3.5 cm from entrance is marked as black squares. (B) A top view of dilution profile averaged over thickness when averaged dilution arrives viewing window(t=6.3s). (C) A side view of dilution profile when t=6.3s. The snap is magnified along z-axis by 10 times for clear view. (D) A cross section view of dilution profile normal to flow direction when t=6.3s.(E) Top view of dilution profile of a layer at the center(z=h/2) of flow chamber when t=6.3s. (F) Top view of dilution profile of a layer one particle radius from substrate (z=a) when t=6.3s.(G) A schematics showing change in adsorbed layer before and after dilution.

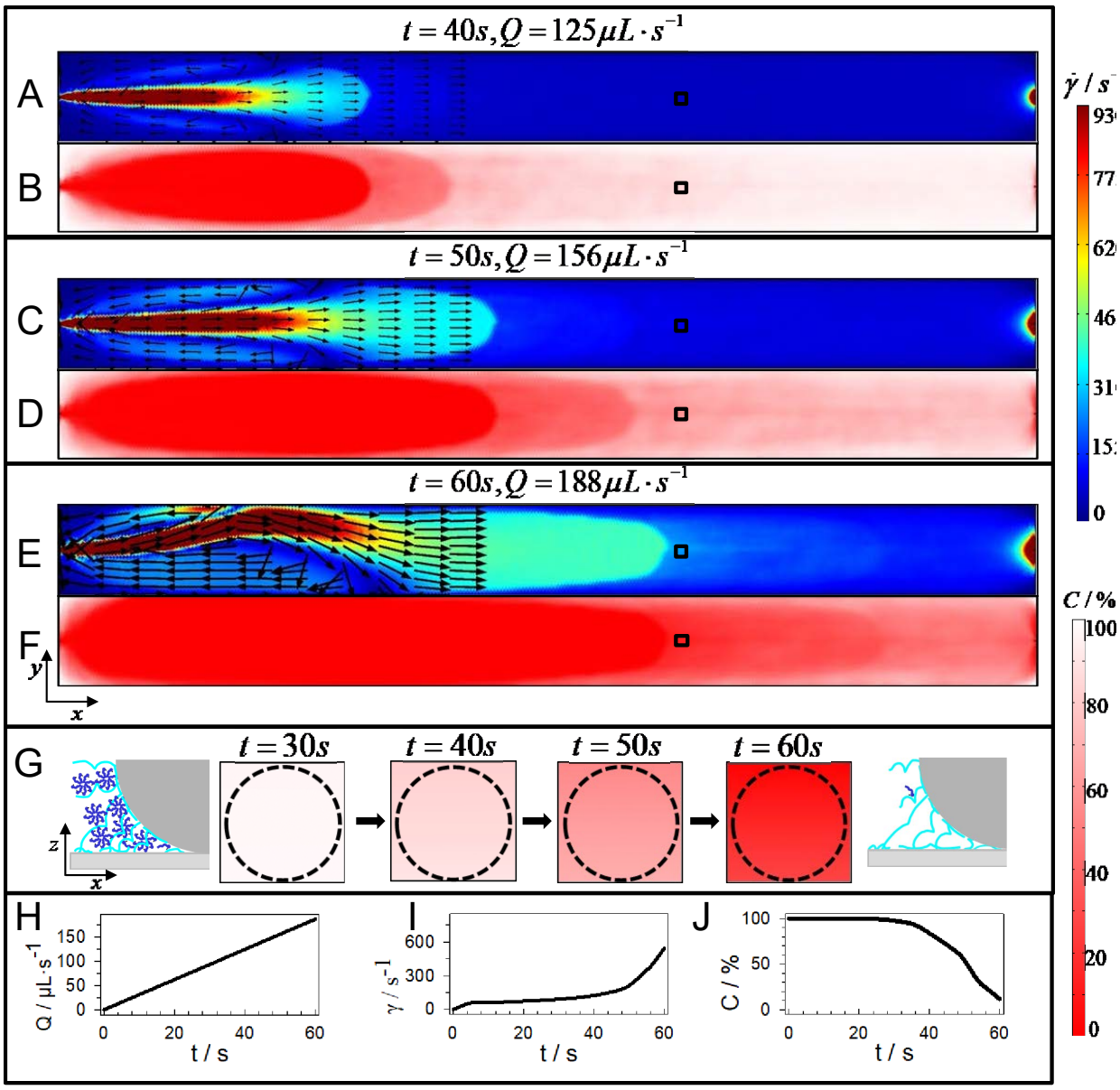

Figure S 9. Dilution and shear rate profile in flow cell for composition D. (A,C,E) Shear rate profile near substrate (z=a) at different time point. Normalized arrows show direction of fluid velocity. **(B,D,F)** Dilution profile near substrate (z=a) at different time point. **(G)** Snaps of dilution process around a deposited particle on side view. **(H)** Flow rate profile from pump programing. **(I)** Shear rate profile at z=a. **(J)** Dilution profile at z=a.

6.5. Original and tracked experimental video

Fig. S10 shows snaps of experiment video observing deposition behavior of particles under shear flow. Fig. S10A is an unprocessed frame at the beginning of video, negatively charged particles with diameter of 6.46μm are deposited on negatively charged glass slide in quiescent fluid with composition A. Although particles with different sizes were studied compared to our previous study, particles were still deposited prior to flow under all four composition tested. This agrees with state diagram (Fig. 5E) proposed by our previous study[17]. Particles with larger size was adapted to better mimic fragrant capsules in personal care product[36], and are more challenging to deposit under shear field.[6]

By tracking trajectory of each particle, deposited particles will be highlighted with different color identifying the origin of their deposition. Red circles represent the particles constantly deposited from the initial frame of video and blue circles highlight particles that had detached and then redeposited on substrate. Particles not highlighted were detached and moving across window.

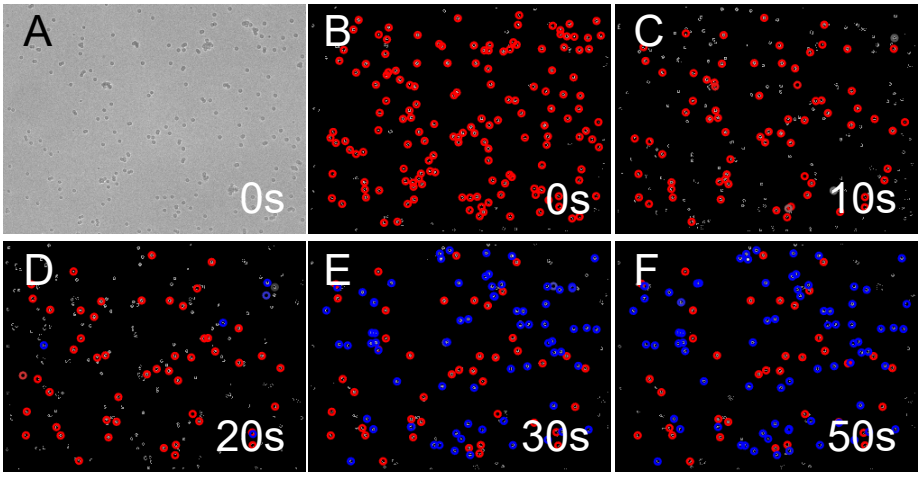

Figure S 10. Snaps of deposited particle being washing off by ramping diluting shear flow and deposit again from flow. (A) Snap of original video before start of flow. **(B-F)** Snaps of tracked video during flow at different time point. Red circles highlight deposited particles from the beginning, blue circles highlight particles deposited from flow. The detached particles are not highlighted and are moving with flow.

Fig. S10B is a frame in tracked video at the same timepoint as in S10A, all particles are deposited and highlighted red unless not tracked. Flow starts after t = 0s together with detachment stage. In Fig. S10C when t=10s, the number of red highlighted particles has significantly decreased. Many detached particles appeared, indicating severe detachment after shear flow. After another 10s, in Fig. S10D, quantity of red circles further decreased. Blue circles started to show up, indicating the start of redeposition stage. Compared with Fig. S10D, Fig. S10E at t=30s has a large increment in number of blue circles. This burst of redeposition behavior of detached particles was observed to last less than 5s. After redeposition stage, there was no more detached particles moving in window thus further deposition cannot be observed. The number of red highlighted and blue highlighted particles both plateaued after deposition stage(Fig. S10F). In the perspective of the general stages observed, this video is representative for the rest of experiments using diluting flow.

6.6. Deposition profile in related with dilution profile

By advancing or postponing viewing point the time in Fig. S11&S12 , the dilution profile can be advanced or postponed. By tracking particle deposition behavior, we found that the end of detachment stage and the start of redeposition stage is advanced or postponed with dilution profile, which showed a strong connection between these two processes.

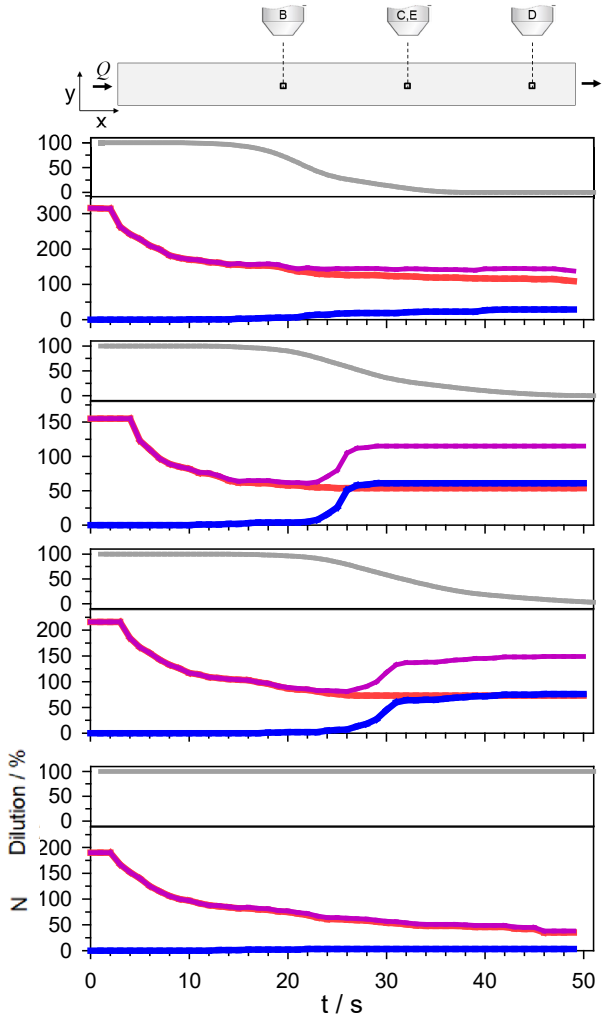

Figure S 11. Correlation of dilution profile and deposition count under different conditions *for composition A*. All four experiments start with composition A (0.00834wt% AAC and 0.2wt% SLES). **(A)** Schematic indicating the position of viewing windows **(B)** Diluting experiment at 2 cm from inlet. **(C)** Diluting experiment at 3.5 cm from inlet. **(D)** Diluting experiment at 5 cm from inlet. **(E)** Non-diluting experiment at 3.5 cm from inlet. Grey lines on top show dilution profile, red line counts deposited particles from initial, blue line counts from flow and purple line sums red line and blue line.

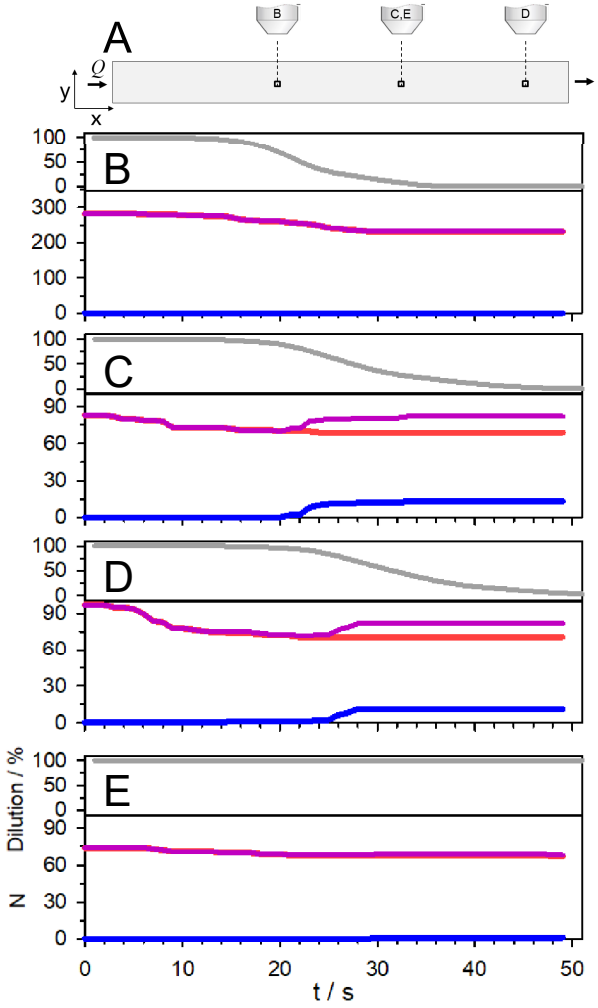

Figure S 12. Correlation of dilution profile and deposition count under different conditions for composition B. All four experiments start with composition A (0.05wt% AAC and 0.2wt% SLES). **(A)** Schematic indicating the position of viewing windows **(B)** Diluting experiment at 2 cm from inlet. **(C)** Diluting experiment at 3.5 cm from inlet. **(D)** Diluting experiment at 5 cm from inlet. **(E)** Non-diluting experiment at 3.5 cm from inlet. Grey lines on top show dilution profile, red line counts deposited particles from initial, blue line counts from flow and purple line sums red line and blue line.

6.7. Schematics for polymer bridges under shear flow

Once shear flow is applied on a deposited particle, particle will rotate slightly until enough displacement that polymer bridges can be stretched. Enough force and torque can be generated to counter detachment. Configuration of polymer layers could be categorized into five regions (Fig. S13). In region I, separation between front of particle and substrate are larger than thickness of undisturbed polymer layer δ_B. Bridges does not form, and polymer chains are at rest. In region II

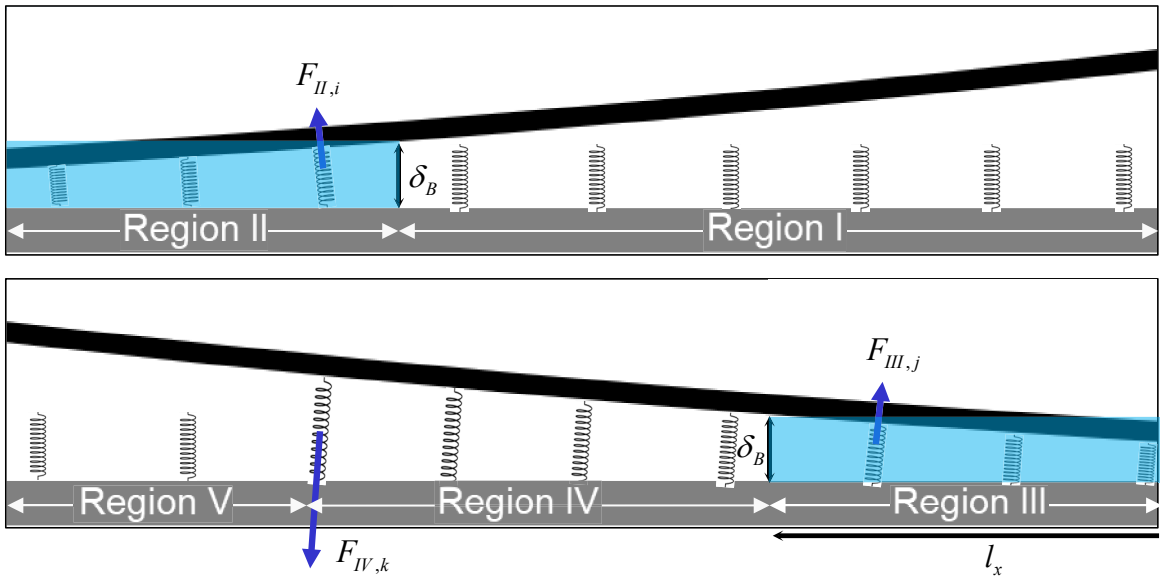

Figure S 13. Schematics of polymer bridging under shear flow. (A) Schematics of polymer bridging in the front of particle. Polymer is at rest and bridges do not form in region I. In region II, separation is smaller than the thickness of an undisturbed polymer. Bridges form and are compressed. **(B)** Schematics of polymer bridging at rear of particle. In region III, Polymer brushes are compressed. In region IV, bridges were stretched. In region V, separation is too large that bridges ruptured.

or III, within a region with length of l_x polymer layer is compressed by particle. Bridges form and exert forces F_{II} or F_{III} on particle resisting compression. F_{II} and F_{III} are symmetrical according to the yz-plane crossing contact point. In region IV, bridges were stretched due to displacement of particle from initial position under shear flow. A force F_{IV} is generated at rear of particle and contribute to deposition. In region V, separation is too large and bridges rupture. Total force in normal and later direction and torque exerted by polymer bridges on particle are,

$$F_B^z = F_{II}^z + F_{III}^z + F_{\mathrm{IV}}^z \tag{28}$$

$$F_B^x = F_{II}^x + F_{III}^x + F_{IV}^x \tag{29}$$

$$T_B = l_I \cdot F_{II}^z + l_{III} \cdot F_{III}^z + l_{IV} F_{IV}^z \tag{30}$$

where l_{II}, l_{III}, l_{IV} are the distance in x between contact point to a polymer in corresponding region. Since region II and III are symmetrical, lateral force and torque can be simplified to,

$$F_B^x = F_{IV}^x \tag{31}$$

$$T_B = l_{IV} \cdot F_{IV}^z \tag{32}$$

Normal bridging force F_B^Z contributes to colloidal force F_A while lateral bridging F_B^x force is referred as friction force F_F and torqueT_B is referred as $T_{A,O}$ in our paper.

6.8. Normal adhesion before and after dilution

In TIRM experiment, elevation of spherical colloids from surface, *h*, could be measured by the intensity of scattered evanescent wave,

$$I(h) = I_0 \exp(-\beta h) \tag{33}$$

where *I* is the scattered intensity, I_0 is contact intensity, and β is decay length of evanescent wave. If the height of particle is observed long enough, its distribution *n(h)* can be converted to potential energy profile *u(h)* with Boltzmann's equation,

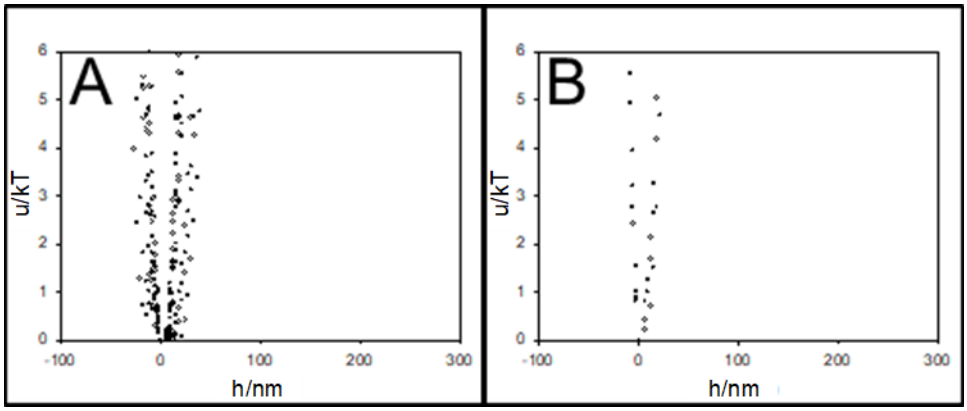

Figure S 14. Potentials of silica particles interacting with negative charged substrate before and after dilution.

$$\frac{u(h)-u(h_0)}{k_BT}=\ln\left[\frac{n(h_0)}{n(h)}\right] \tag{34}$$

where h_0 is a reference height usually chosen as the most probably height.

In Fig. S14, potential profile of deposited particles is obtained before and after dilution of composition A. As can been seen, attraction well obtained before dilution is wider than after dilution, which means normal adhesion is higher after dilution. This agrees with flow cell experiment, after dilution, deposited particles could resist detachment by higher shear rate than before.

7. REFERENCES

1. Kronberg, B.; Holmberg, K.; Lindman, B., *Surface chemistry of surfactants and polymers*. John Wiley & Sons: 2014.
2. Coughlan, A. C. H.; Torres-Diaz, I.; Jerri, H. A.; Bevan, M. A., Direct Measurements of kT-Scale Capsule–Substrate Interactions and Deposition Versus Surfactants and Polymer Additives. *ACS Applied Materials & Interfaces* **2018,** *10* (32), 27444-27453.
3. Miyake, M., Recent progress of the characterization of oppositely charged polymer/surfactant complex in dilution deposition system. *Advances in Colloid and Interface Science* **2017,** *239*, 146-157.
4. Goldman, A.; Cox, R.; Brenner, H., Slow viscous motion of a sphere parallel to a plane wall—II Couette flow. *Chemical engineering science* **1967,** *22* (4), 653-660.
5. Saffman, P., The lift on a small sphere in a slow shear flow. *Journal of fluid mechanics* **1965,** *22* (2), 385-400.
6. Burdick, G.; Berman, N.; Beaudoin, S., Describing hydrodynamic particle removal from surfaces using the particle Reynolds number. *Journal of Nanoparticle research* **2001,** *3* (5-6), 453-465.
7. Rabinovich, E.; Kalman, H., Incipient motion of individual particles in horizontal particle–fluid systems: B. Theoretical analysis. *Powder Technology* **2009,** *192* (3), 326-338.
8. Jadhav, S.; Eggleton, C. D.; Konstantopoulos, K., A 3-D computational model predicts that cell deformation affects selectin-mediated leukocyte rolling. *Biophysical journal* **2005,** *88* (1), 96-104.
9. Dasanna, A. K.; Fedosov, D. A.; Gompper, G.; Schwarz, U. S., State diagram for wall adhesion of red blood cells in shear flow: from crawling to flipping. *Soft matter* **2019,** *15*

(27), 5511-5520.
10. Moshaei, M. H.; Tehrani, M.; Sarvestani, A., On Stability of Specific Adhesion of Particles to Membranes in Simple Shear Flow. *Journal of Biomechanical Engineering* **2018,** *141* (1).
11. Ryu, B. K.; Hommel, R. J.; Roberts, P.; Fréchette, J., Promoting rotation, friction, and mixed lubrication for particles rolling on microstructured surfaces. *Physical Review E* **2019,** *99* (2), 022802.
12. Ryan, J. N.; Elimelech, M., Colloid mobilization and transport in groundwater. *Colloids and Surfaces A: Physicochemical and Engineering Aspects* **1996,** *107*, 1-56.
13. Kuo, S. C.; Hammer, D. A.; Lauffenburger, D. A., Simulation of detachment of specifically bound particles from surfaces by shear flow. *Biophysical Journal* **1997,** *73* (1), 517-531.
14. Belyaev, A. V., Long ligands reinforce biological adhesion under shear flow. *Physical Review E* **2018,** *97* (4), 042407.
15. Kalasin, S.; Santore, M. M., Sustained Rolling of Microparticles in Shear Flow over an Electrostatically Patchy Surface. *Langmuir* **2010,** *26* (4), 2317-2324.
16. Bhat, R. R.; Genzer, J.; Chaney, B. N.; Sugg, H. W.; Liebmann-Vinson, A., Controlling the assembly of nanoparticles using surface grafted molecular and macromolecular gradients. *Nanotechnology* **2003,** *14* (10), 1145.
17. Najafi, H.; Jerri, H. A.; Valmacco, V.; Petroff, M.; Hansen, C.; Benczédi, D.; Bevan, M. A., Synergistic Polymer-Surfactant Complex Mediated Colloidal Interactions & Deposition. *ACS Applied Materials & Interfaces* **2020**.
18. Lee, J.-J.; Fuller, G. G., Adsorption and desorption of flexible polymer chains in flowing systems. *Journal of Colloid and Interface Science* **1985,** *103* (2), 569-577.
19. Cohen, Y., Hydrodynamic thickness of adsorbed polymers in steady shear flow. *Macromolecules* **1988,** *21* (2), 494-499.
20. Kaneko, D.; Narita, T.; Gong, J. P.; Osada, Y.; Ando, J.; Yamamoto, K.; Ohnishi, S.; Yaminsky, V., Thickness decrease of a grafted polyelectrolyte membrane exposed to shear flow. *Journal of Polymer Science Part B: Polymer Physics* **2003,** *41* (22), 2808-2815.
21. Varga, I.; Mezei, A.; Mészáros, R.; Claesson, P. M., Controlling the interaction of poly(ethylene imine) adsorption layers with oppositely charged surfactant by tuning the structure of the preadsorbed polyelectrolyte layer. *Soft Matter* **2011,** *7* (22), 10701-10712.
22. Nakamura, K.; Shikata, T., Small Angle Neutron Scattering Study of Polyelectrolyte Conformation Incorporated into Hybrid Threadlike Micelles under Strong Shear Flows. *The Journal of Physical Chemistry B* **2007,** *111* (43), 12411-12417.
23. Liberatore, M. W.; Wyatt, N. B.; Henry, M.; Dubin, P. L.; Foun, E., Shear-Induced Phase Separation in Polyelectrolyte/Mixed Micelle Coacervates. *Langmuir* **2009,** *25* (23), 13376-13383.
24. Dubin, P. L.; Li, Y.; Jaeger, W., Mesophase Separation in Polyelectrolyte-Mixed Micelle Coacervates. *Langmuir* **2008,** *24* (9), 4544-4549.
25. Chen, Y. M.; Katsuyama, Y.; Gong, J. P.; Osada, Y., Influence of Shear Stress on

Cationic Surfactant Uptake by Anionic Gels. *The Journal of Physical Chemistry B* **2003,** *107* (49), 13601-13607.

26. Ilekti, P.; Piculell, L.; Tournilhac, F.; Cabane, B., How To Concentrate an Aqueous Polyelectrolyte/Surfactant Mixture by Adding Water. *The Journal of Physical Chemistry B* **1998,** *102* (2), 344-351.
27. Bali, K.; Varga, Z. f.; Kardos, A.; Varga, I.; Gilányi, T.; Domján, A.; Wacha, A. s.; Bóta, A.; Mihály, J.; Mészáros, R. b., Effect of dilution on the nonequilibrium polyelectrolyte/surfactant association. *Langmuir* **2018,** *34* (48), 14652-14660.
28. Braem, A. D.; Biggs, S.; Prieve, D. C.; Tilton, R. D., Control of persistent nonequilibrium adsorbed polymer layer structure by transient exposure to surfactants. *Langmuir* **2003,** *19* (7), 2736-2744.
29. Dedinaite, A.; Claesson, P. M.; Bergström, M., Polyelectrolyte− surfactant layers: adsorption of preformed aggregates versus adsorption of surfactant to preadsorbed polyelectrolyte. *Langmuir* **2000,** *16* (12), 5257-5266.
30. Dedinaite, A.; Claesson, P. M., Interfacial properties of aggregates formed by cationic polyelectrolyte and anionic surfactant. *Langmuir* **2000,** *16* (4), 1951-1959.
31. Mohr, A.; Nylander, T.; Piculell, L.; Lindman, B.; Boyko, V.; Bartels, F. W.; Liu, Y.; Kurkal-Siebert, V., Mixtures of Cationic Copolymers and Oppositely Charged Surfactants: Effect of Polymer Charge Density and Ionic Strength on the Adsorption Behavior at the Silica–Aqueous Interface. *ACS Applied Materials & Interfaces* **2012,** *4* (3), 1500-1511.
32. Jamieson, E. J.; Fewkes, C. J.; Berry, J. D.; Dagastine, R. R., Forces between oil drops in polymer-surfactant systems: Linking direct force measurements to microfluidic observations. *Journal of Colloid and Interface Science* **2019,** *544*, 130-143.
33. Svensson, A. V.; Johnson, E. S.; Nylander, T.; Piculell, L., Surface Deposition and Phase Behavior of Oppositely Charged Polyion−Surfactant Ion Complexes. 2. A Means to Deliver Silicone Oil to Hydrophilic Surfaces. *ACS Applied Materials & Interfaces* **2010,** *2* (1), 143-156.
34. Wang, W.; Johnson, E. S.; Nylander, T.; Ellingson, P.; Schubert, B.; Piculell, L., Selective co-deposition of anionic silica particles at hydrophobic surfaces from formulations of oppositely charged polymers and surfactants. *Journal of colloid and interface science* **2016,** *467*, 213-219.
35. Stanimirova, R. D.; Kralchevsky, P. A.; Danov, K. D.; Xu, H.; Ung, Y. W.; Petkov, J. T., Oil drop deposition on solid surfaces in mixed polymer-surfactant solutions in relation to hair-and skin-care applications. *Colloids and Surfaces A: Physicochemical and Engineering Aspects* **2019,** *577*, 53-61.
36. Jerri, H. A.; Jacquemond, M.; Hansen, C.; Ouali, L.; Erni, P., "Suction Caps": Designing Anisotropic Core/Shell Microcapsules with Controlled Membrane Mechanics and Substrate Affinity. *Advanced Functional Materials* **2016,** *26* (34), 6224-6237.

37. Maddar, F. M.; Perry, D.; Brooks, R.; Page, A.; Unwin, P. R., Nanoscale Surface Charge Visualization of Human Hair. *Analytical Chemistry* **2019,** *91* (7), 4632-4639.
38. Saffman, P., Corrigendum to'The lift on a small sphere in a slow shear flow'. *J. Fluid Mech.* **1968,** *31*, 624.
39. Goldman, A. J.; Cox, R. G.; Brenner, H., Slow viscous motion of a sphere parallel to a plane wall—I Motion through a quiescent fluid. *Chemical engineering science* **1967,** *22* (4), 637-651.
40. Eichmann, S. L.; Meric, G.; Swavola, J. C.; Bevan, M. A., Diffusing colloidal probes of protein–carbohydrate interactions. *Langmuir* **2013,** *29* (7), 2299-2310.
41. Edwards, T. D.; Bevan, M. A., Polymer Mediated Depletion Attraction and Interfacial Colloidal Phase Behavior. *Macromolecules* **2012,** *45* (1), 585-594.
42. Cosgrove, T.; Mears, S.; Obey, T.; Thompson, L.; Wesley, R., Polymer, particle, surfactant interactions. *Colloids and Surfaces A: Physicochemical and Engineering Aspects* **1999,** *149* (1-3), 329-338.
43. Jha, B.; Cueto-Felgueroso, L.; Juanes, R., Fluid mixing from viscous fingering. *Physical review letters* **2011,** *106* (19), 194502.
44. Wild, J. D.; Potter, O. E., A falling liquid film on a sphere. *The Chemical Engineering Journal* **1972,** *4* (1), 69-76.
45. King, M. R.; Hammer, D. A., Multiparticle adhesive dynamics: Hydrodynamic recruitment of rolling leukocytes. *Proceedings of the National Academy of Sciences* **2001,** *98* (26), 14919-14924.
46. Huang, P.; Guasto, J. S.; Breuer, K. S., Direct measurement of slip velocities using three-dimensional total internal reflection velocimetry. *Journal of fluid mechanics* **2006,** *566*, 447-464.

VITA

EDUCATION

Johns Hopkins University, Baltimore, United States 09/2018-present
M.SCI.ENG Degree expected in 2020, Major in Chemical &Biomolecular Engineering
Overall GPA: 3.9/4.0 | TOEFL: 105 | GRE: V155+Q169+AW3.5
Soochow University, Suzhou, China 09/2014-06/2018
B.ENG Degree Received in 2018, Major in Chemical Engineering
Overall GPA: 3.6/4.0 Rank 2/35
Summer Session at **University of California-Berkeley** 06/2016-08/2016

PUBLICATIONS

- **Zhang, L. (first)**; Bevan, M. "Colloidal deposition versus shear and polymer/surfactant composition" in preparation
- Tian, X.; **Zhang, L. (co-first)…** Pan; Y. "Functional Magnetic Hybrid Nanomaterials for Biomedical Diagnosis and Treatment." *Wiley Interdisciplinary Reviews Nanomedicine & Nanobiotechnology* (2017). DOI: 10.1002/wnan.1476. Citation: 37
- Pan, Y.; …**Zhang, L.** …"Metal-based Hybrid Nanomaterials as Radiosensitizers in Cancer Radiotherapy". *Colloids and Interface Science Communications.* 10.1016/j.colcom.2018.01.004. Citation: 13

RESEARCH EXPERIENCES

Prof. Michael. A. Bevan Lab

Grad Researcher, Supervisor: Prof. Michael. A. Bevan 10/2018-Present

- Studied Colloid Deposition via Synergistic Surfactant-Polymer Interactions
- Studied the effect of shear, dilution and polymer/surfactant composition on particle deposition

Suzhou Key Laboratory of Green Chemical Engineering
Undergraduate Researcher, Supervisor: Dr. Zhangxiong Wu 09/2017-06/2018

- Proposed a method for controllable synthesis of mesoporous carbon material doped with cobalt, and its application in hydrogen addition catalysis

State and Local Joint Engineering Laboratory for Novel Functional Polymeric Materials
Undergraduate Researcher, Supervisor: Dr. Yue Pan, Dr. Xin Tian 10/2015-06/2017

- Developed a magnetic-based system applying superparamagnetic iron oxide and a magnetic field gradient to exert a force on these particles for drug targeting applications
- Studied the design and synthesis of MHNs (Magnetic Hybrid Nanomaterials) and their applications as multimodal imaging probes and therapy agents in biomedicine

INDUSTRIAL EXPERIENCE

Dow Chemical Zhangjiagang Co Ltd, Site Logistics, Intern 07/2018-08/2018

- Project leading in designing and manufacturing ISO-tank manlid bolt thightening tool

Dow Corning Zhangjiagang Co Ltd, Production Department, Intern 07/2015-08/2015

- Identified the effects of operating variables (operating pressure, operating temperatures, and properties of heat exchanger) on heat exchanger performance in grinder area
- Participated in the installation of heat exchangers and accessories

SKILLS

- Software: MATLAB, COMSOL, Sigmaplot, Putty, MestReNova, ChemBioDraw
- Techniques: TIRM, video microscopy, microfluidics, FTIR, NMR, TEM, SEM, GPC, HPLC, TGA, XPS, XRD